UPPSALA UNIVERSITET

FYSMAS1037

Examensarbete 30 hp
Oktober 2015

Simulating the spectra of galaxies in the reionization epoch

Constraining the escape fraction of ionizing photons

Christian Binggeli

Masterprogrammet i fysik
Master Programme in Physics

UPPSALA UNIVERSITET

Teknisk- naturvetenskaplig fakultet
UTH-enheten

Besöksadress:
Ångströmlaboratoriet
Lägerhyddsvägen 1
Hus 4, Plan 0

Postadress:
Box 536
751 21 Uppsala

Telefon:
018 – 471 30 03

Telefax:
018 – 471 30 00

Hemsida:
http://www.teknat.uu.se/student

Abstract

Simulating the spectra of galaxies in the reionization epoch

Christian Binggeli

The cosmic reionization represents a fundamental yet poorly understood phase transition in the evolution of our universe. The most promising theory is that the ionizing radiation from young hot stars in star-forming galaxies drove reionization, but much information about the number of galaxies and the escape fraction of ionizing radiation from galaxies is still missing. In this thesis, I discuss a technique for estimating the escape fraction of hydrogen ionizing radiation from galaxies in the reionization epoch. The method utilizes the power law slope of the UV continuum and the equivalent width of the Balmer beta emission line to try to estimate the escape fraction of a galaxy from its spectrum without ever directly observing any ionizing radiation. The technique is applied to simulated galaxies from large scale cosmological simulations.

I find that the method works for estimates of the escape fraction of dust free simulated galaxies. It is possible to distinguish between galaxies with escape fractions 0.0, 0.5, 0.7 and 0.9 when no dust is added to the galaxies. I also show that the method works regardless of choice of numerical assumptions and assumptions about stellar evolution in the models. Lastly, I show that the addition of dust to the galaxies can introduce an ambiguity to the estimated escape fraction, and that this may reduce the estimation into just being between high or low escape fractions. The results also show that equivalent widths of the Balmer beta emission line larger than approximately 100 Ångströms are seen only in galaxies with escape fractions consistent with zero. The addition of dust and its effect on the spectral features used in the technique allows for an estimation of the average dust content. I find that the galaxies contain low amounts of dust, with a highest average dust attenuation in the visual of A=0.4-0.6 magnitudes.

Handledare: Erik Zackrisson
Ämnesgranskare: Kjell Olofsson
Examinator: Andreas Korn
FYSMAS1037

Popular science summary in Swedish

Populärvetenskaplig sammanfattning på svenska

Vårt universum har befunnit sig i många olika stadier under sin utveckling. En period som är viktig men som vi inte ännu förstår fullt ut är den kosmiska återjoniseringen. Denna period inleddes när de första stjärnorna och galaxerna bildades, och ledde till det universum fyllt av tunn joniserad gas som vi ser omkring oss idag. Under återjoniseringen övergick gasen som fyllde universum från att vara neutral till joniserad när energirik joniserande strålning delade upp de neutrala atomerna i gasen till atomkärnor och elektroner, dvs. joner och elektroner. Källan till den joniserande strålningen är inte helt fastställd, men mycket av dagens forskning pekar på att strålningen som drev den kosmiska återjoniseringen kom från unga heta stjärnor i stjärnbildande galaxer. Det fanns också andra källor som kunde bidra med joniserande strålning, men forskning på området visar att de inte kan ha bidragit med majoriteten av de joniserande fotoner som krävdes för att jonisera gasen mellan galaxerna. Genom att man har uteslutit andra källor till den joniserade strålningen har stjärnbildande galaxer klivit fram som de främsta kandidaterna. Anledningen att man främst diskuterar stjärnbildande galaxer är att det är där man finner de yngsta och hetaste stjärnorna; den typ av stjärnor som avger mest joniserande strålning.

Observationer av kvasarer och den kosmiska bakrundsstrålningen pekar på att den kosmiska återjoniseringen pågick under en period cirka 300-900 miljoner år efter big bang. Detta begränsade tidsintervall gör att man kan definiera två villkor som galaxerna måste uppfylla för att kunna ha drivit återjoniseringen. Dels måste det finnas tillräckligt många stjärnbildande galaxer, och dels måste tillräckligt mycket joniserande strålning kunna ta sig ut ur galaxerna. Neutral gas och stoft i galaxerna kan nämligen absorbera den joniserande strålningen från stjärnorna, och således hindra den från att ta sig ut.

Man kan fastställa antalet stjärnbildande galaxer som bidrog med joniserande strålning genom att man gör observationer. För att göra detta krävs metoder och teleskop som tillåter att man observerar även ljussvaga galaxer, då de skulle kunna ha bidragit med en signifikant mängd joniserande fotoner (om antalet ljussvaga galaxer är stort). Att lista ut hur mycket joniserande strålning som läcker ut ur galaxerna är något mer komplicerat. Den neutrala gasen runtomkring galaxerna gör det omöjligt att direkt observera hur mycket strålning som läcker ur galaxer under återjoniseringen. Det finns dock sätt att kringgå detta. Man kan till exempel titta på närbelägna galaxer och se hur mycket joniserande strålning som läcker ut ur dem och sedan extrapolera detta till de avlägsna galaxer som joniserade universum. Man kan också simulera dessa avlägsna galaxer och försöka dra slutsatser från simuleringar. Den metod som diskuteras i denna uppsatsen utgör ett tredje sätt att undersöka antalet läckande joniserande fotoner. Metoden baseras på att man med hjälp av signaturer i galaxers spektrum kan uppskatta andelen av joniserande fotoner (f_{esc}) som lyckas ta sig ut ur galaxerna. I uppsatsen har metoden testats med hjälp av avancerade simuleringar av de galaxer som tros ha joniserat universum.

Jag har tillämpat metoden på simulerade stoftfria galaxer för att se om det är möjligt att använda de utvalda särdragen för att uppskatta antalet läckande joniserande fotoner. Resultatet av detta är att det går att göra en uppskattning av f_{esc} med hjälp av de särdrag som har valts ut. Samtidigt visar det sig att vissa simuleringar tillåter betydligt noggrannare bestämning av denna andel. Detta beror troligtvis på hur galaxens stjärnbildningshistoria har sett ut och hur mycket metaller galaxerna innehåller. I uppsatsen visar jag även att metoden inte är beroende av särskilda numeriska antaganden eller antaganden gällande hur stjärnorna utvecklas, utan den fungerar även när man ändrar dessa (inom rimliga gränser).

Jag har även undersökt hur stoft påverkar vissa delar av galaxernas spektrum. Stoft kan nämligen blockera joniserande strålning, och hindra den från att läcka ut ur galaxen. Det minskade antalet joniserande fotoner som lyckas ta sig ut ur galaxen gör att galaxens spektrum ser annorlunda ut. Effekten av stoft är systematisk, och man bör kunna kompensera för stoftets påverkan på spektrat. Dock tillåter inte de simulerade galaxer som har använts i min studie att man gör en sådan kompensation. Detta beror troligtvis på att stoftmängden är för låg för att påverka spektrumet så mycket att en kompensation kan göras.

Det har varit möjligt att göra uppskattningar på övre gränsen av stoftinnehåll hos stjärnbildande galaxer vid cirka 800 miljoner år efter big bang. Resultaten visar på att dessa galaxer troligtvis inte innehöll mycket stoft, något som stämmer väl överens med observationella studier av galaxer av denna typ. För övrigt är det i enlighet med teorin om att dessa galaxer inte är speciellt utvecklade, och att de inte ännu har berikats med de tyngre grundämnen som behövs för att bilda betydande mängder stoft.

Resultaten från min studie skulle kunna användas som grund för observationella studier av galaxer under återjoniseringsprocessen. De kan ge en fingervisning om vilka särdrag som är intressanta att titta på och vilka galaxer som man kan tillämpa metoden på. Till exempel skulle denna uppsats kunna ligga som grund för en förstudie på hur man kan använda det framtida James Webb-teleskopet för att observera galaxer under återjonieringseran och uppskatta andelen av joniserande fotoner som lyckas ta sig ur dem.

Vidare studier skulle kunna ägna sig åt att använda större delar av spektrumet för att uppskatta andelen av fotoner som tar sig ut ur galaxerna. Kanske skulle hela spektrumet kunna användas. Detta skulle i princip vara möjligt genom att man till exempel utnyttjade så kallad “*machine learning*” för att lära datorer att identifiera galaxer med olika f_{esc}. Med hjälp av detta skulle man kunna göra avsevärt noggrannare analyser av spektra och på så sätt komma närmare att besvara frågan om hur det intergalaktiska mediet återjoniserades, och hur universum blev vad det är idag.

Acknowledgements

I would like to express my deep gratitude to my supervisor Erik Zackrisson. He has been everything you could ask for in a supervisor (and more). Without his expertise, openness and support, this thesis would never have been. Kjell Olofsson deserves thanks for acting as my secondary supervisor. In addition to that, his general uplifting personality and slightly odd jokes has made the work with my master thesis so much more fun. I would like to thanks my friends and family for providing moral support, proof reading and for listening to my monologues about galaxies, the universe and bugs in my computer code. I owe special thanks to Stefan Book, for many long conversations, long walks and evenings spent drinking tea. You have been a true friend. Lastly, I would like to thank my partner Linnéa Jantvik for so many things, not least for being the most supportive partner I could ever have wished for. Thank you.

Contents

1 Introduction **1**

2 Theoretical background **5**
2.1 Escape mechanisms of Lyman continuum radiation 6
2.2 Dust 7
2.3 Cosmological simulations 9

3 Calculation of SEDs of galaxies at z$\sim$ 7 **11**
3.1 Selection of spectra 12

4 Results **14**
4.1 The EW(Hβ)-β diagram without dust 14
4.2 The effect of dust on the EW(Hβ)-β diagram 18
4.2.1 The Finlator et al. (2006) dust recipe 21
4.2.2 Gaussian dust distributions 26
4.2.3 The Bergvall et al. (2015) dust recipe 29
4.2.4 The Shimizu et al. (2014) dust recipe 32

5 Conclusions **35**

1. Introduction

The universe has gone through many different stages of evolution before ending up the way we observe it today. One important phase that still remains to be fully understood is the period in which the neutral hydrogen in the universe became ionized. This event is called the cosmic reionization. Observations of the cosmic microwave background (CMB) together with observations of quasars have constrained the reionization process to have taken place between redshift $z \sim 14$ and $z \sim 6$ (Zahn et al. 2012). While there is a generally favoured theory to explain the cosmic reionization process, which is that the reionization was driven by leakage of hydrogen ionizing radiation (Lyman continuum radiation; LyC) from galaxies, observations have not been able to study this in any detail. The question is whether the amount of Lyman continuum radiation escaping from galaxies at $z \geqslant 6$ is enough to sustain a reionized intergalactic medium (IGM) at a given time. The main problem in answering this question is that there have thus far been no reliable observational techniques to estimate the amount of LyC that escaped the galaxies in the reionization epoch. The increasingly neutral IGM as we approach the end of the reionization makes it impossible to observe the actual leakage of LyC, as the neutral gas in the IGM absorbs basically all radiation at the relevant wavelengths (Inoue et al. 2014). However, there may be techniques that allow us to indirectly determine the LyC escaping from galaxies at $z \geqslant 6$ without ever actually observing the LyC photons. A first step towards developing such a technique was taken by Zackrisson et al. (2013), and the aim of this project is to further develop the technique. This will be done by applying the method to realistic galaxies from large-scale cosmological simulations (Smoothed particle hydrodynamics; SPH, and Adaptive mesh refinement; AMR), in contrast to the slightly simplified models used in Zackrisson et al. (2013).

In order to estimate the contribution from galaxies, there are two main questions that have to be answered. We need to determine the number of galaxies that may have contributed to the ionization process, as well as the ionizing luminosity of these galaxies (Finlator 2012). The first question is one of observational tools. While the contribution from currently detectable galaxies at $z = 6$ is estimated as not being enough to sustain ionization, there is missing data at the faint end of the galaxy luminosity function (Robertson et al. 2010, 2013). The contribution from the faint end of the galaxy population may be enough to sustain reionization, but this requires a large enough number of faint galaxies that are below current observational limits. New and better observational facilities and techniques may help in solving this problem by simply pushing the limit of what can be observed.

The second question is: How large is the ionizing luminosity of each galaxy, or how many ionizing photons does each galaxy release into the IGM? This is directly connected to the amount of gas in and around the galaxy that is able to absorb the ionizing photons before they escape into the IGM. Of course, the ionizing luminosity also depends on the age and metallicity of the stellar populations of galaxies, as well as the amount of dust present in the surroundings of each galaxy. The effect of dust, age and metallicity on the spectral energy distributions (SED) and the outcome of the technique will be addressed in this thesis as well. The absorption of photons in the gas in the galaxy leaves a signature in the SED. Basically this means that spectral features may be used to estimate the ionizing luminosity even in cases where the gas significantly affects some fraction of this radiation (Zackrisson et al. 2013).

This is the main idea behind the technique discussed in this paper, that the amount of ionizing radiation escaping (escape fraction f_{esc}) from galaxies can be inferred from their SEDs. Some of the ionizing photons (rest frame wavelength $\leqslant 912$ Å) produced inside galaxies get absorbed in the surrounding neutral hydrogen gas. As the ionized hydrogen recombines, the energy may be emitted as multiple UV/optical (or longer wavelength) photons as the electron cascades through the shells of the hydrogen atom. Thus, the ionizing photons effectively get reprocessed into nebular continuum flux at longer wavelengths or into emission lines. By studying the UV/optical parts of the SEDs of galaxies, information can be extracted about the fraction of LyC photons that escape (f_{esc}) the galaxy, and that are able to reionize the IGM (Zackrisson et al. 2013). Methods for estimating the *typical* escape fraction of LyC in the reionization epoch using fluctuations in the cosmic infrared background have been proposed (Fernandez et al. 2013). However, so far, the method discussed in Fernandez et al. (2013) has not yet been used to estimate the escape fraction of reionization epoch galaxies. Attempts have also been made to determine the escape fraction using photometric methods, for example by Ono et al. (2010), Bergvall et al. (2013), Pirzkal et al. (2012) and Pirzkal et al. (2013). The technique described in this thesis hopes to produce more reliable results by using spectrometry instead of photometry. While Jones et al. (2013) have presented a spectroscopic in which metal absorption lines have been used, the method presented there is only able to place an upper limit to the escape fraction of LyC. Our method should be able to place both upper and lower limits by using other spectral features to estimate f_{esc}.

To be able to estimate the produced/escaping amount of hydrogen ionizing photons, two spectral features are used; the slope of the UV continuum (power-law slope β; $f_\lambda \propto \lambda^\beta$) and the equivalent width EW(Hβ) of the Balmer β emission line. The reprocessing of photons into nebular continuum flattens the UV slope, making the continuum redder. So, a lower escape fraction leads to a flatter (redder) UV slope, while a higher escape fraction leads to a steeper (bluer) UV slope. The equivalent width of Hβ is affected in a similar way — a larger fraction of escaping photons produces smaller EW(Hβ) while a smaller fraction of escaping photons produces larger EW(Hβ) (Zackrisson et al. 2013). In practice, this should allow for estimation of the fraction of escaping hydrogen ionizing photons without ever having to directly measure the ionizing flux of the galaxies. There are, however some factors that may cause problems when attempting to infer the escaping fraction of photons. Age, metallicity and dust have an impact on the SEDs of galaxies, and cause reddening of the spectra (Zackrisson et al. 2008, 2013). This reddening may make the galaxy appear as if it had a different escape fraction, introducing a possible ambiguity to the result.

One of the goals of this study is to apply the method to four different sets of simulated galaxies (Finlator et al. 2013; Shimizu et al. 2014; Paardekooper et al. 2013, 2015; Gnedin & Kaurov 2014; Gnedin 2014). Another issue that will be addressed in this study is how the results are affected by assumptions made in the technique. In practice, this is a question of how spectra are chosen for stars of different ages and metallicity during the calculation of the galaxy spectrum. The attenuation of radiation by dust is the third and final part of this study. Here, I will attempt to describe how dust affects the results of the technique, and what correction for dust that works best.

Studies have found a correlation between the UV luminosity and the slope β of $z \sim 7$ galaxies. Fainter galaxies seem to have bluer β, while more luminous galaxies seem to have redder β (Bouwens et al. 2014). This of course makes the study and detection of more faint high redshift galaxies even more important, as the bluer β means that they have a high ionizing luminosity. Furthermore, the observed behaviour of β suggests that these galaxies have low dust extinction (Bouwens et al. 2014). Faint galaxies may therefore have SEDs which are significantly less affected by dust, and may thus be better candidates to consider when attempting to use the technique discussed in this thesis.

The method could be applied to real galaxies if sufficiently good spectra can be obtained. Zackrisson et al. (2013) argue that the method could be used to identify $f_{esc} \geqslant 0.5$ galaxies up to redshift $z \approx 9$ using the *Near Infrared Spectrograph (NIRSpec)* upcoming *James Webb Space Telescope (JWST)*. By selecting galaxies that are subject to strong gravitational lensing effects (and therefore appear brighter), spectra of galaxies can be obtained for $M_{1500} \lesssim -16.0$ galaxies at $z \sim 7$ and for $M_{1500} \lesssim -17.5$ galaxies at $z \sim 9$ (Zackrisson et al. 2013).

In section 2 I will discuss the theoretical background to the project. The mechanisms which allow ionizing radiation to escape from galaxies will be discussed in section 2.1, dust and its impact on galaxies as well as observational studies on the dust in galaxies will be discussed in section 2.2. In section 2.3, the simulations from which the galaxies were obtained will be briefly discussed. Section 3 discusses the method used to estimate the escape fraction of ionizing radiation from the galaxies. In this section, I will also focus a bit on the numerical properties and the assumptions going into the method (section 3.1).

In section 4 I will discuss the results of applying the method onto the simulated galaxies. This section will be split into two main parts. In the first part (section 4.1) I will discuss the results of the method when used on dust-free galaxies from the simulations. In the second part (section 4.2), I will discuss four different recipes for dust attenuation.

The recipe by Finlator et al. (2006) is discussed in section 4.2.1, Bergvall et al. (2015) in section 4.2.3 and Shimizu et al. (2014) in section 4.2.4. I will also discuss a recipe for handling dust that simply assigns a dust attenuation to a galaxy's stars according to a Gaussian distribution centred around some value in section 4.2.2.

Finally I will interpret the results to draw conclusions about galactic properties of reionization epoch galaxies and what kind of studies that could follow up this thesis in section 5.

2. Theoretical background

The questions about the number of galaxies and their ionizing luminosities discussed in section 1 are basically what needs to be answered in order to determine the impact of galaxies on reionization. There has been much work done on the reionization process and the contribution of reionizing photons from galaxies. Much of the work implies that the galaxy population present at those redshifts ($z \sim 6$) could in principle be enough to sustain a reionized intergalactic medium (Bouwens et al. 2012b; Robertson et al. 2013; Finkelstein et al. 2012a). However, as mentioned in section 1, there is missing data at the faint end of the galaxy luminosity function. What is meant by this is that the number of faint galaxies in the reionization epoch is currently unknown, and thus their contribution to the ionizing luminosity is hard to estimate. If there are many faint galaxies present in the reionization epoch, these could add up to a considerable ionizing flux which can in turn account for the missing ionizing flux needed to sustain reionization.

This is a problem that could only be circumvented by using new observational facilities or techniques that allow us to probe galaxies at lower luminosities than is currently possible. Meanwhile, simulations can point us in the right direction, and there have been simulations that point toward galaxies as the main driver behind reionization. Simulations by Ciardi et al. (2003) have produced results for galaxy driven reionization which agree well with observations of the cosmic microwave background by the WMAP spacecraft. In their study, they do not find the need to include exotic objects like very massive stars or miniquasars for the simulations to agree with observational data from WMAP. More recently Robertson et al. (2015) have been able to match multiple parameters of their galaxy driven reionization models to CMB radiation data from the Planck spacecraft.

However, even if the there is a large number of galaxies that may contribute to reionization, the ionizing radiation must be able to escape from these to be able to ionize the IGM. Therefore, one of the important discussions on the ionizing flux of galaxies in the reionization epoch is the escape fraction of ionizing photons. Direct measurements of escaping LyC radiation have been made for galaxies in the local universe (Bergvall et al. 2006; Leitet et al. 2011, 2013; Borthakur et al. 2014), and there are more recent studies that present evidence for escaping LyC at ~ 3 (Vanzella et al. 2015; Siana et al. 2015; de Barros et al. 2015). However, as mentioned earlier, the neutral hydrogen gas at reionization rules out direct detection of LyC from galaxies at redshift $z \sim 7$. The method proposed in this thesis circumvents this problem, but the mechanisms that govern the release of LyC into the IGM still have to be understood in order for us to draw any conclusions from the application of the method. One important factor to consider is the way in which the ionizing radiation is leaking, and how the morphology of the galaxy may affect this (anisotropic leakage etc.). The dust in galaxies may also play an important part when it comes to restricting the release of ionizing photons.

It is worth mentioning that, while the generally accepted theory is that the stars inside galaxies were the main contributors of ionizing photons at redshifts $z > 6$, there are other objects that do produce ionizing photons and significantly contribute to the ionizing photon budget in recent times. Active galactic nuclei (AGN) and quasars have been considered as possible sources for ionizing radiation at $z > 6$. While AGN are able to sustain a fully ionized IGM by themselves at low redshift ($z < 3$), observations show that the contribution from AGN is insufficient at larger redshift (Cowie et al. 2009). Quasars also contribute significantly to the number of ionizing photons in the low-z universe, but the number of quasars present at $z > 6$ cannot account for the photons required to sustain reionization at that time. Estimates by Willott et al. (2010) show that the contribution from quasars to the hydrogen ionizing photon budget at $z = 6$ is far too low, accounting only for $1 - 5\%$ of the required flux.

2.1. Escape mechanisms of Lyman continuum radiation

The fraction of ionizing photons that are able to escape from galaxies depends in many ways on the shape and morphology of a galaxy. Certain conditions are required for a LyC photon to be able to escape the galaxy in which it originates. The path that the photon travels must be free from neutral hydrogen, or else it will be absorbed. This is possible either if the photon path is clear of gas, or if the hydrogen gas through which the photon travels is ionized. The first case means that there are holes in the nebula surrounding the stars in a galaxy. These holes can form as powerful winds from OB stars and supernovae blow away gas, and form cleared '*bubbles*' around themselves large enough to penetrate out of the neutral hydrogen (HI) region in a galaxy (Mac Low & McCray 1988). A nebula in which the ionizing radiation is only able to partly ionize the the hydrogen is called a ionization bounded nebula, and as mentioned above, these nebulae require holes if LyC is to escape from them.

The heightened rate of supernovae in a star forming region may lead to a larger amount of gas being cleared, which allows more ionizing radiation to escape. This clearing can be affected by the position and distribution of star forming regions. The effect of having decentralized star formation in clusters is studied in Clarke & Oey (2002). Their model shows that the clearing of gas is significantly affected by the distribution of star forming regions, and that the escape fraction is increased when the star formation is decentralized. This result is maybe not totally unexpected, as distributions where star formation is taking place near the edge of the galaxy lead to larger escape fractions, due to lower gas column density.

A case that is related to holes in the HI region is clumping of the HI gas in the ISM. If the gas is clumped, there will of course be regions where the optical depth of LyC is smaller. Fernandez & Shull (2011) study the possible connection between the distribution of clumps, the density of the clump/interclump medium and the escape fraction. They find that the covering factor and the density of the clump/interclump medium significantly affects the escape fraction of LyC photons.

Another way in which the ionizing photons can escape galaxies is if the hydrogen gas around the stars is fully ionized, and the LyC flux is powerful enough to overcome the recombination rate of the hydrogen, allowing ionizing photons to escape through the ionized gas. In this case the nebula is said to be density-bounded (Zackrisson et al. 2013). Strong starbursts may for example produce so much ionizing radiation, that the nebula in the region is totally ionized, allowing LyC photons to escape. In Leitherer et al. (1996), a central starburst region in NGC4214 was observed using the Hubble telescope (HST). The authors argue that this region is density-bounded to the ionizing radiation. Studies have also found evidence that so called "Green Pea"-galaxies at redshift $z \sim 0.1 - 0.3$ may be density bounded (Jaskot & Oey 2013).

The galaxy Haro 11 was the first local galaxy from which escape or LyC was observed (Bergvall et al. 2006). The galaxy was first thought to have a density-bounded nebula, due to the galaxy's low neutral hydrogen content. However, Bergvall et al. (2006) argue that the neutral hydrogen is still enough to lead to gas column densities that are too high for LyC to escape. The prevailing mechanism thus seems to be holes in the nebula that allows LyC to escape.

However, it could be the case that more complex morphologies are possible. There could be galaxies in which a nebula that combine the properties of radiation bounded and density bounded nebulae.

There is, however, a third mechanism which can lead to increased escape fractions, but which is not connected directly to the degree of ionization of the interstellar medium (ISM) or to the density or porosity of the HI gas in the galaxy. Migrating stars could end up at the outer regions of galaxies where the gas column density is lower, and more of LyC is able to escape. In Conroy & Kratter (2012), the authors discuss the effect of runaway stars in high redshift galaxies. In the relatively small galaxies at high redshifts, migrating stars could migrate far from the dense central regions of the galaxy, which would enhance the effect of migrating stars in high redshift galaxies compared to galaxies today. Conroy & Kratter (2012) produce models in which the inclusion of runaway stars leads to higher escape fractions. The authors claim that this implies that the runaway stars may contribute with $50\% - 90\%$ of the total ionizing radiation escaping from high redshift galaxies.

2.2. Dust

The attenuation of radiation by dust can pose a problem when attempting to estimate the escape fraction using the method described in this thesis. The light emitted in the

UV (rest-frame) from star forming galaxies in the local universe that is absorbed in the interstellar dust is re-emitted at the far-infrared part of the spectrum (Adelberger & Steidel 2000). This reprocessing of UV photons into longer wavelength photons can effectively remove information about the escape fraction from the SED by altering the spectral features used to estimate the escape fraction.

However, since galaxies in the reionization epoch are relatively young, there is a chance that they have not yet experienced substantial metal enrichment and thus contain relatively small amounts of dust. Many studies of reionization-epoch galaxies point toward a seemingly small extinction in these galaxies $A_v \lesssim 0.2$ mag (Finkelstein et al. 2012b; Bouwens et al. 2012a; Dunlop et al. 2012b; Wilkins et al. 2013). Earlier studies by Bouwens et al. (2009, 2011) seem to point toward negligible extinction in galaxies at redshift $z > 7$. Meanwhile, there have been studies performed that question this view. Schaerer & de Barros (2010) present results from analysing redshift $z \sim 6-8$ galaxies discovered by COSMOS and HST and their dust attenuation using broad-band photometry. Their results seem to point to a considerably larger extinction in galaxies at redshifts $z \approx 6-8$, with values ranging up to $A_v \approx 1$ mag. An observational study performed earlier this year by Watson et al. (2015) shows evidence of dusty galaxies at these high redshifts. The galaxy in question was spectroscopically determined to be at redshift $z = 7.5 \pm 0.2$, and is a star forming galaxy. Meanwhile, the galaxy is highly evolved, rich in dust content and has a large stellar mass. Watson et al. (2015) argue that this does show that there are in fact dusty and evolved galaxies among the fainter star forming galaxies at these redshifts. A recent study by Mancini et al. (2015) also points to the possibility of dust rich galaxies at high redshift, and that efficient grain growth is the dominating contributor to dust mass in massive galaxies at $z \geqslant 6$.

In Zackrisson et al. (2013), some distributions and their effects on the spectral features are outlined. The authors focus mainly on two distributions, an ionization-bounded nebula with a dust screen, and a ionization-bounded nebula where dust and ionized hydrogen are mixed. In both cases, the nebulae have holes through which unattenuated direct star light can escape. In the case of the dust screen, the attenuation has an effect on the UV slope β but almost no effect on EW(Hβ) for low escape fractions, since the stellar continuum emerging from the screen dominates the rest-frame UV. At high escape fractions, the pure stellar light dominates over the attenuated radiation, and thus the UV slope β is less affected while EW(Hβ) decreases. For the case with gas and dust mixed in the galaxy, Zackrisson et al. (2013) apply a very simplified model, in which half the attenuation takes place before the stellar light can interact with the nebula, and the other half after the nebular absorption/emission. As pointed out by the authors, this is a very simplified model, but serves to exemplify the trends of β and EW(Hβ). The trend in this case is that the galaxies move toward higher (redder) UV slopes β and smaller EW(Hβ) regardless of the escape fraction.

2.3. Cosmological simulations

Large scale cosmological simulations provide a unique way to study large structures and processes in the universe. The increase in computational power over the last ~ 20 years has allowed simulations like these to be used for many purposes, not least the study of galaxies, their properties and their contribution to reionization (Shimizu et al. 2011, 2012; Paardekooper et al. 2013; Finlator et al. 2013; Gnedin 2014; Shimizu et al. 2014; Paardekooper et al. 2015). Of course, any good simulation should be able to reproduce observational quantities, and galaxies calculated using these kinds of simulations have been compared to observed galaxies, and seem to reproduce certain quantities well (Shimizu et al. 2011, 2012; Finlator et al. 2013; Gnedin 2014).

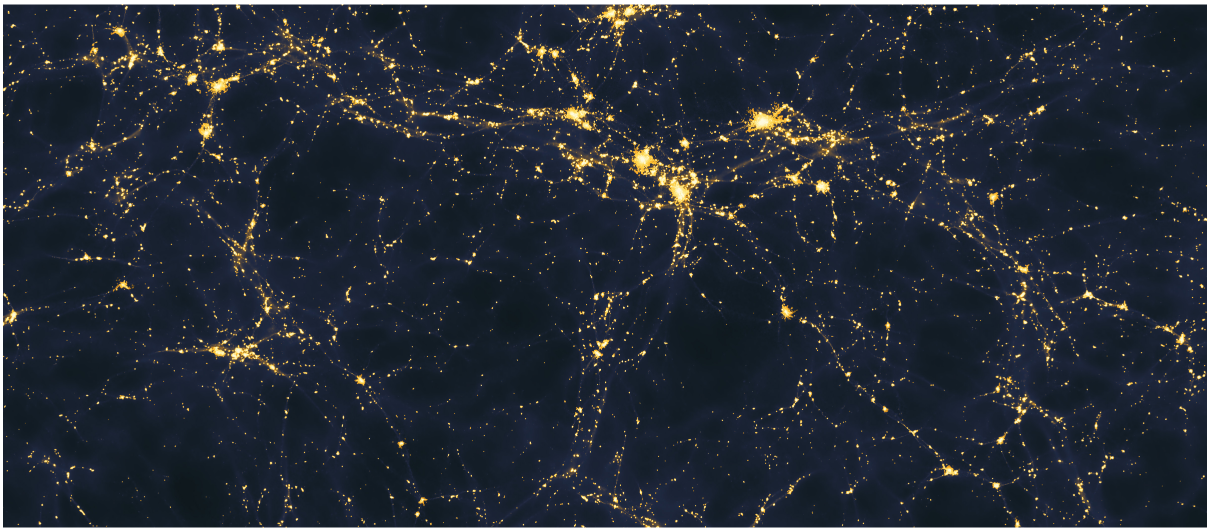

Figure 1: The figure shows a computer simulation of the type that is discussed in this thesis. The image is more than 50 million lightyears across, and shows the large scale distribution of galaxies in the universe. One can clearly see the cosmic web of gas, galaxies and dark matter that makes up the universe. Image credit: Andrew Pontzen and Fabio Governato.

In this thesis, four different sets of cosmological simulations will be used to model the escape of LyC radiation from high redshift galaxies. The simulations used are those by Finlator (Finlator et al. 2013), Shimizu (Shimizu et al. 2014), Paardekooper (Paardekooper et al. 2013, 2015) and Gnedin (Gnedin & Kaurov 2014; Gnedin 2014). These simulations have previously been used to study galaxies and their properties, and have been compared to observational quantities. Results from the simulations by Gnedin have shown good agreement with observational data of the high-redshift Lyman α (Lyα) forest and the abundance of Lyα emitters (Gnedin 2014). The simulations by Finlator et al. (2013) have been used to study OI absorbers at redshift $z \sim 6$, where they find a marginal agreement with OI absorbers abundance observed at those redshifts. The simulations by Shimizu have been used to model submillimetre galaxies and Lyman alpha emitters, in both cases the simulations reproduce statistical quantities of observed galaxies (Shimizu et al. 2011, 2012). The simulated galaxies by Shimizu also reproduce the UV luminosity function from $z \sim 7$ to $z \sim 10$. Furthermore, they also reproduce the observed UV slope distribution (Shimizu et al. 2014).

The simulations model galaxy formation, evolution and the reionization process inside a limited volume. The volume starts off containing only gas and dark matter. As regions of increased density appear, stars and galaxies are formed. In order to model these processes, many physical mechanisms have to be considered, such as star formation, stellar feedback, reionization etc. (Paardekooper et al. 2013; Finlator et al. 2013; Gnedin & Kaurov 2014; Shimizu et al. 2014; Paardekooper et al. 2015). From the simulation volume, it is possible to extract information about the galaxies that are present at a certain time. For this study, the galaxies are selected during reionization, so at redshift $z \sim 7$. We are thus able to use these large scale simulations to extract the mass, metallicity and age of collections of stars inside the galaxies that contributed to the cosmic reionization. This information can then be used to calculate spectral properties of the galaxies. Ideally, one would want to know the mass, metallicity and age of every single star within a simulated galaxy, but due to computational limitations, the resolution is limited to clusters of stars, or "*star particles*".

The simulations by Finlator et al. (2013); Shimizu et al. (2014); Paardekooper et al. (2013, 2015) are based on the same SPH (Smoothed particle hydrodynamics) code, GADGET (*GAlaxies with Dark matter and Gas intEracT*) (Springel et al. 2001; Springel 2005). The simulations by Gnedin & Kaurov (2014); Gnedin (2014) are based on a different method than the above mentioned simulations. Instead, their simulations use the *Adaptive Refinement Tree* (ART) (Kravtsov et al. 1997, 2002; Rudd et al. 2008), which utilizes an adaptive refinement mesh method. A detailed discussion of the above mentioned simulations is outside of the scope of this study. For such discussions, see Springel et al. (2001); Springel (2005); Finlator et al. (2013); Shimizu et al. (2014); Paardekooper et al. (2013, 2015); Gnedin & Kaurov (2014); Gnedin (2014).

3. Calculation of SEDs of galaxies at z~ 7

From the cosmological simulations discussed in section 2.3, we extract information about the mass, metallicity and age of the star particles in each galaxy in the simulation volume. To obtain a spectrum for a galaxy, we thus need to have spectra for star particles of arbitrary mass, age and metallicity where stellar continuum, nebular continuum and nebular emission lines have been included. Using an initial mass function, the spectral synthesis code Yggdrasil (Zackrisson et al. 2011) produces these spectra for star particles by summing the spectra of single stars while considering the mass distribution from the stellar initial mass function. In this thesis, the spectra for single-age populations for population I and II stars come from Starburst99 (Leitherer et al. 1999; Vázquez & Leitherer 2005), and are generated using both Padova-AGB and Geneva stellar evolutionary tracks. For population III and extremely metal poor (EMP) stars, the spectra by Raiter et al. (2010) are used. The photoionization code Cloudy (Ferland et al. 1998) is used to add nebular continuum and nebular emission lines onto the purely stellar spectrum from Yggdrasil. At this point, we have the spectra of single-age star particles required to calculate the spectrum of a galaxy. This is done using the LYCAN code. In this code, the spectra of single-age star particles are combined using the star formation history from the simulations to account for arbitrary star formation within the galaxy. In this step, the nebular contribution to the spectrum is weighted depending on the escape fraction of the galaxy, such that galaxies with smaller escape fraction receive a larger contribution from nebular emission lines and nebular continuum and vice versa. Note that here, there is no direct consideration of the geometry or morphology of the galaxy, the model does not consider this, but rather just adds a nebular contribution which corresponds to a certain escape fraction.

However, it is not guaranteed that the cosmological simulations produce star particles which perfectly match the age and metallicity of those available from Yggdrasil. In fact, most (if not all) star particles will not perfectly match any of the star particles for which spectra are available. Therefore, some selection in age and metallicity must be performed. How this selection is done and the effect of the selection on the spectra of the galaxies will be discussed in section 3.1.

From the spectrum produced in LYCAN, it is possible to extract information about the spectral features, such as the power law slope β and the equivalent width of the Balmer β line EW(Hβ). Calculating the UV slope β can be done in various ways. In this thesis, the slope β is calculated using the definition of β by Calzetti et al. (1994). This means that the slope is calculated using the overall flux (both nebular and stellar) in a rest-frame wavelength range $1268 - 2580$ Å. To avoid interference from stellar and interstellar absorption features, the wavelength range is split into 10 intervals. This, together with the equivalent width of the Balmer β line allows us to construct the EW(Hβ)-β diagram

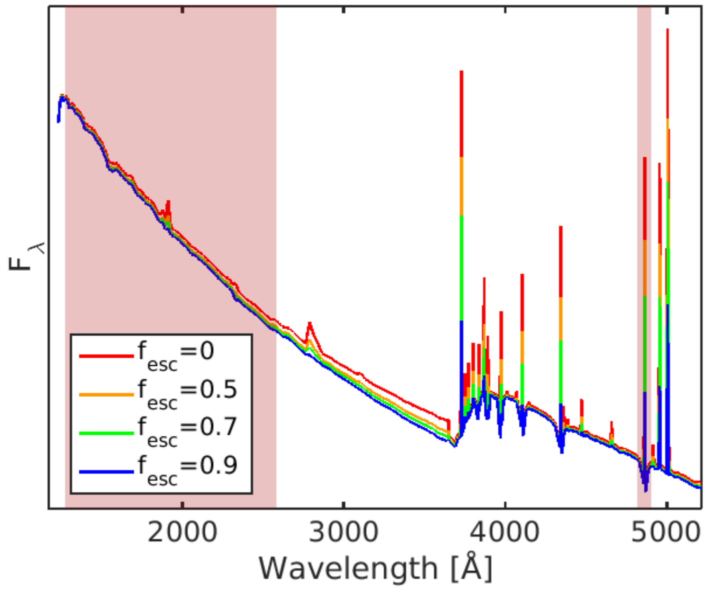

Figure 2: The spectrum of a simulated galaxy (Finlator simulation set) where different escape fractions have been applied to the same galaxy to highlight the effect of the escape fraction on the spectrum. The figure shows shows the galaxy for escape fraction 0.0 *(red)*, 0.5 *(yellow)*, 0.7 *(green)* and 0.9 *(blue)*. The highlighted areas show the spectral features (UV slope β and Hβ) used to estimate the escape fraction.

seen in figure 2, where the abscissa shows the equivalent width of the Balmer β line and the ordinate shows the UV slope β. As mentioned in section 1, the addition of a nebula onto a young stellar population will shift the emission in the red-ward direction. This means that the expected effect of smaller escape fractions is a flatter UV slope β and hence larger values of β. The effect can be seen in figure 2, where the galaxies with higher escape fractions generally show lower (steeper) UV slopes β.

Observations of the UV slopes of high redshift galaxies studies have found UV slopes around $\langle\beta\rangle \approx -2$ (McLure et al. 2011; Dunlop et al. 2012a; Bouwens et al. 2014; Watson et al. 2015). This value allows us to test the simulated galaxies to see if they reproduce the observed beta slopes. This could also provide a test for the dust attenuation, since the addition of dust to the galaxies is expected to lead to redder spectra. Assuming that the simulated galaxies reproduce properties of real galaxies fairly well, it should be possible to place an upper limit on the dust content in the galaxies given the observed UV slopes.

3.1. Selection of spectra

The way in which the parameters of star particles are matched to spectra from Yggrasil could have a significant impact on the resulting EW(Hβ)-β diagram. Tests of different selection methods are performed to determine the effects of the galaxy population spectrum. A grid of spectra of different ages and metallicities was created using Yggdrasil. From this grid, the spectra for star particles of different ages and metallicities are selected. The simplest selection method is a "*nearest neighbour*" selection, where the spectrum for the closest matching metallicity and age is chosen without considering the next closest match to the star particle metallicity and age.

Another selection method is to use a linear interpolation in age and metallicity. This means that the resulting spectrum is a weighted mean of four different spectra. The final selection method that was tested was a linear interpolation in logarithmic age and metallicity. This can be motivated by the fact that these quantities span several orders of magnitude. A comparison between the different methods can be seen in figure 3.

What can be seen is that the *nearest neighbour* method produces slightly redder galaxies than the two interpolation methods. The effect is not large, and the choice of selection method seems not to affect the result in any significant way. Nevertheless, the interpolation in logarithmic age and metallicity was chosen as the main selection method to be used throughout the project.

Since the Starburst99 spectra are available for both Geneva and Padova-AGB evolutionary tracks, a comparison of these was made to determine the possible effects that the choice of evolutionary models could have on the resulting EW(Hβ)-β diagram. The same cosmological simulation was used while choosing spectra calculated by either Geneva or Padova-AGB evolutionary tracks. The comparison can be seen in figure 4. In both cases, pop III and EMP stars come from Raiter et al. (2010). It is apparent that using the Geneva evolutionary model produces significantly redder galaxies. There seems to be no significant difference in EW(Hβ). There is, however a slight difference in the spread of the galaxies. The Geneva evolutionary models do produce a smaller spread in the diagram. For the rest of the thesis, the Geneva evolutionary tracks in combination with the Raiter et al. (2010) evolutionary tracks for pop III and EMP stars will be used to calculate all spectra of galaxies. Thus, choosing evolutionary models from Padova-AGB would produce generally bluer galaxies ($\Delta\beta \approx 0.05$) than the galaxies shown in the results of this thesis.

To see how a single galaxy evolves in the EW(Hβ)-β diagram, ten mock galaxies were created for testing purposes. These galaxies have the same mass and metallicity, but the age of the SPH particles is varied. By varying the age, a track can be plotted that shows how the galaxy evolves in the EW(Hβ)-β diagram (using Padova evolutionary tracks). Figure 5a shows this diagram. Furthermore, the effect of interpolating in log age is also studied more thoroughly using the same method. Spectra for the ten test galaxies were obtained once while using the nearest neighbour approach and once while interpolating in log age (figure 5b). The ages for the galaxies were chosen in such a way so that their ages is somewhere in the middle between the ages for which spectra are available. Note that the difference is very small.

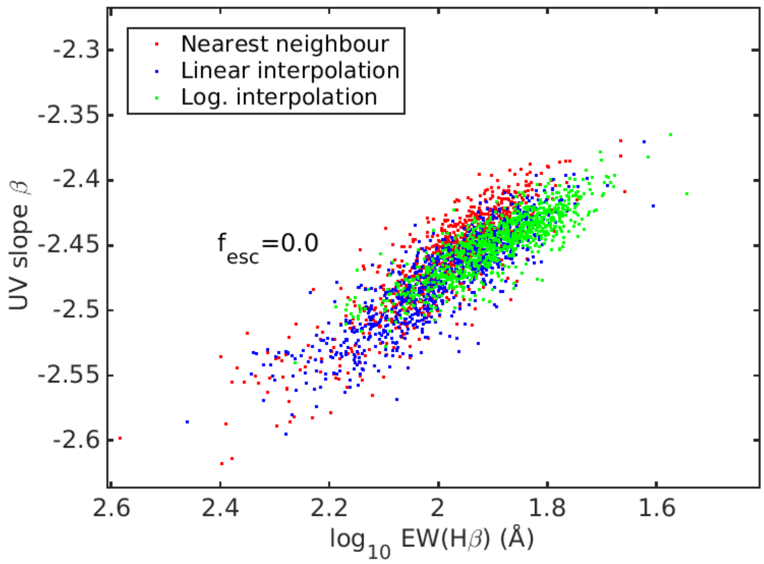

Figure 3: The EW(Hβ)-β diagram showing $\sim$ 800 galaxies subject to three different interpolation schemes. The galaxies shown come from the Gnedin simulation (redshift $z \sim 7$) and have masses $M_\star \geqslant 10^7$. The escape fraction is 0.0 for all galaxies. The colors represent three different methods for selecting SEDs of star particles. *Nearest neighbour* (*red*), linear interpolation in age and metallicity (*blue*) and interpolation in log age and log metallicity (*green*).

4. Results

The method described in section 3 was applied to all selected galaxies from the four simulation sets. The procedure was first performed while ignoring dust and any effects of dust attenuation on the SED's of the galaxies (section 4.1) and then while considering dust (section 4.2). The effect of dust on the SED's was calculated using multiple dust recipes and attenuation laws (see section 4.2).

4.1. The EW(Hβ)-β diagram without dust

The resulting EW(Hβ)-β diagrams are shown in figure 7. There, the galaxies are plotted for four different escape fractions $f_{esc} = 0.0, 0.5, 0.7, 0.9$. What can clearly be seen is that galaxies with similar escape fractions have similar spectral features, and thus form groups according to their escape fractions. This grouping is especially clear in the case of the Gnedin simulations, which show a very small spread in EW(Hβ)-β. In the Shimizu and Finlator simulations it is fairly straightforward to distinguish the groups in the case of blue β slopes and large EW(Hβ). But as the UV slope becomes flatter and the

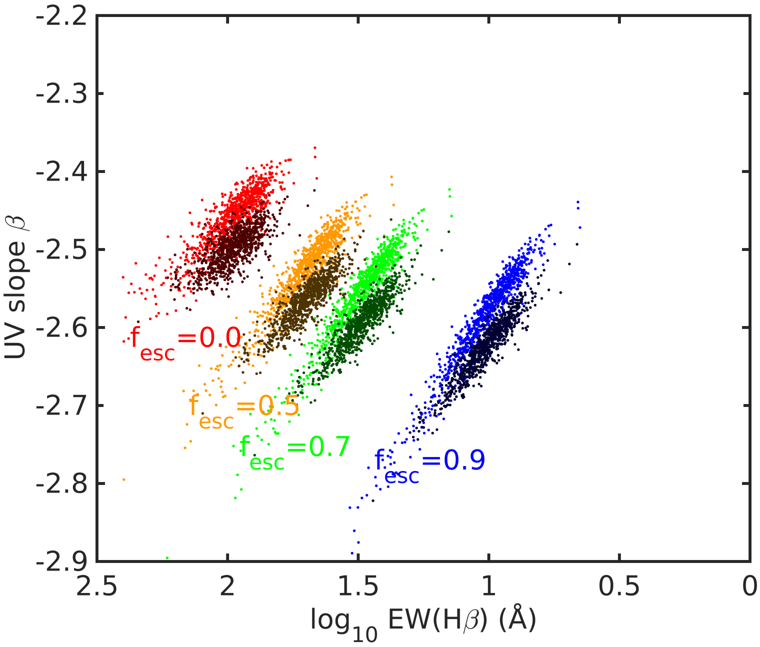

Figure 4: The resulting β vs EW(Hβ) diagram for comparison between Geneva and Padova stellar evolutionary tracks. The brighter *(red, yellow, green, blue)* points represent galaxies where SEDs for star particles come from Geneva evolutionary tracks, while the darker points *(dark red, dark yellow, dark green, dark blue)* represent galaxies where SEDs come from Padova evolutionary tracks. All galaxies are at $z \sim 7$ and are from the simulation by Gnedin.

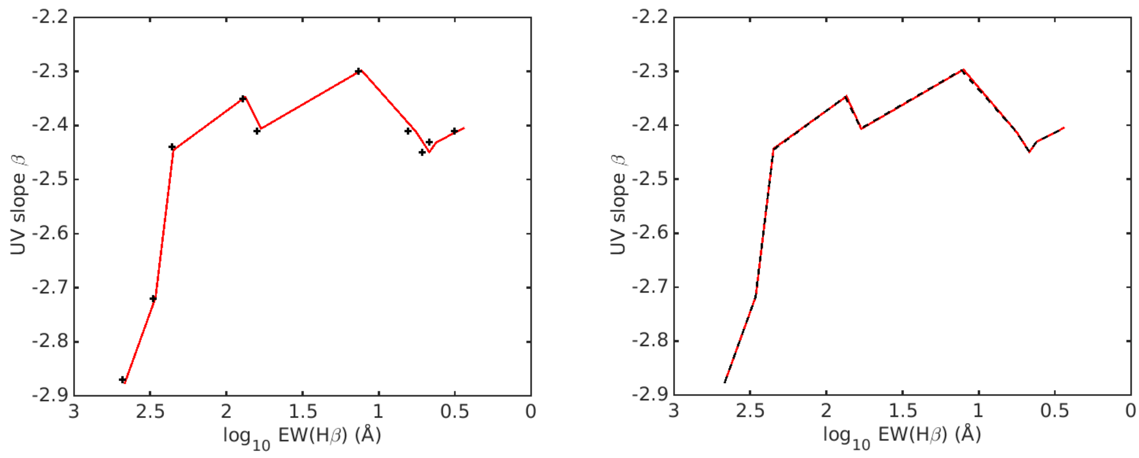

Figure 5: *(a)* A comparison between the evolution in the EW(Hβ)-β diagram of an instantaneous burst population from the Yggdrasil code and the evolution of a test instantaneous burst population (or mock galaxy) for which the SED has been calculated using the procedures outlined in this thesis. The metallicity of both populations is $Z = 0.02$, and both have escape fraction $f_{esc} = 0.0$. The ages of the test population are $1.5, 2.5, 3.5, 4.5, 5.5, 6.5, 7.5, 8.5, 9.5, 10.5$ Myr, while the ages from the Yggdrasil population are $\sim 1, 2, 3, 4, 5, 6, 7, 8, 9, 10$ Myr. *(b)* A comparison between the test population plotted once while using the nearest neighbour method *(dashed, black)* and once interpolating in log age *(red)*. In both these tests, the Padova evolutionary tracks were used.

equivalent width of the Balmer β line decreases, the galaxies become mixed up, making the determination of the escape fraction ambiguous.

The Gnedin simulations do not exhibit this behaviour, nor do they show an increase in spread when moving to larger β and smaller EW(Hβ). Furthermore, the overall scatter of the Gnedin simulations is smaller than in the Finlator and Shimizu galaxies (the Paardekooper simulations are excluded from this discussion due to the limited number of galaxies in that set). Possible explanations for this may be a smoother star formation history (SFH) in the Gnedin models and a smaller spread in metallicity.

A comparison between the SFH of the Gnedin, Shimizu and Finlator simulated galaxies can be seen in figure 8. The star plots show the normalized star formation rate for 100 galaxies, with the Gnedin galaxies exhibiting the smallest spread and the Finlator galaxies the largest. This means that the stellar population in the Gnedin galaxies will have similar age distributions, which may explain the similarity in the spectral features. Furthermore, the Gnedin simulated galaxies also show a small spread in metallicity (see figure 9). Since the metallicity of the galaxies has an impact on the SED, a more narrow spread in metallicity may lead to more similar spectra. These effects are expected to produce galaxies which have a smaller spread in the EW(Hβ)-β diagram. However, I expect that the SFH effect dominates, and that the metallicity effect is significantly smaller.

From figure 9, it is also apparent that the galaxies from the different simulations vary significantly in metallicity. The Paardekooper simulations produce galaxies with a factor of ten larger metal content than the Gnedin galaxies.

A simple test for this was done by synthesising 20 Gnedin galaxies and using fixed values for either age or metallicity of the particles in the simulation. The result of this comparison can be seen in figure 6. Metallicity and age both affect the spread, but they do so differently. When the age is fixed, the galaxies line up along a central line which corresponds to the escape fraction. From this, it seems likely that the SFH is the dominating factor when it comes to the spread of the Gnedin galaxies, and that while there is a contribution from metallicity, the main effect comes from the smooth SFH of the Gnedin models.

The UV slope β for the simulated dust free galaxies lies below the value observed in many studies (McLure et al. 2011; Dunlop et al. 2012a; Bouwens et al. 2014). This indicates that some amount of dust attenuation must be present. As expected, the UV slope β becomes steeper as the escape fraction increases, which is explained by a larger stellar contribution to the UV part of the spectrum.

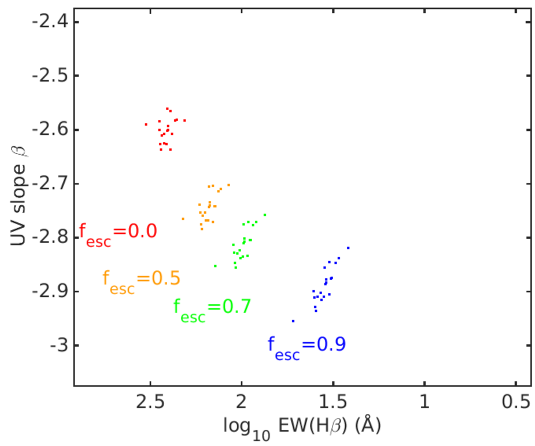

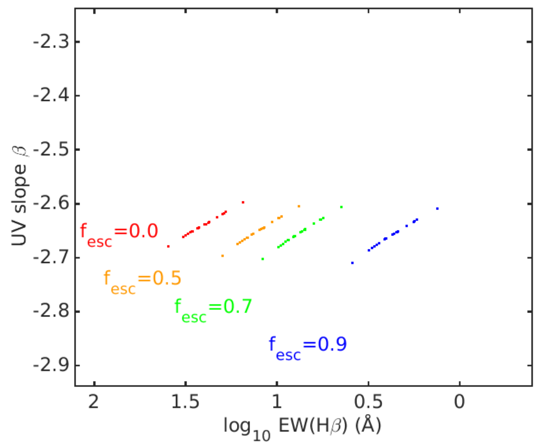

Figure 6: EW(Hβ)-β diagram showing the same 20 dust free galaxies from the Gnedin simulation set plotted once for constant metallicity *(left)* and once with constant age *(right)* of SPH particles. The figure illustrates how the metallicity and age of SPH affects the spread of the galaxies in the EW(Hβ)-β diagram. Escape fractions: 0.0 (red), 0.5 (yellow), 0.7 (green) and 0.9 (blue). Note that the figure is only to exemplify the behaviour of the spread of the galaxies, and that the positions of the galaxies in the diagram is not relevant as this depends on what constant metallicity and age that is chosen. What can be seen is that both metallicity and age do effect the spread of the galaxies in the EW(Hβ)-β diagram.

4.2. The effect of dust on the EW(Hβ)-β diagram

The method discussed in this thesis hinges on the fact that galaxies of certain escape fractions can be effectively distinguished from galaxies of other escape fractions. Dust will no doubt cause a reddening on the spectrum of the galaxy. Whether this reddening rules out the possibility to distinguish galaxies of different escape fractions is, however unclear. Depending on the distribution and density of the dust in the galaxy, the spectral features will be affected differently.

There are different ways in which the dust attenuation for a given galaxy can be calculated. In our case, the color excess $E(B-V)$ is calculated according to some recipe. In this thesis, a total of four different recipes for dust attenuation were used: Finlator et al. (2006), Bergvall et al. (2015), Shimizu et al. (2014) and a Gaussian dust distribution.

Using the color excess, a number of different reddening curves were implemented to further study the impact of dust attenuation on the galaxy spectrum, and the effect of dust attenuation on the resulting EW(Hβ)-β diagram. The reddening curves used were the Calzetti et al. (2000) reddening law, once implemented as it is presented in Calzetti et al. (2000) and once by letting the stellar and nebular component suffer the same extinction, and the Pei (1992) Large Magellanic Cloud (LMC) and Small Magellanic Cloud (SMC) attenuation laws (figure 10). Note that the Calzetti law is implemented in these two ways because there is evidence to suggest that the Calzetti law can lead to an

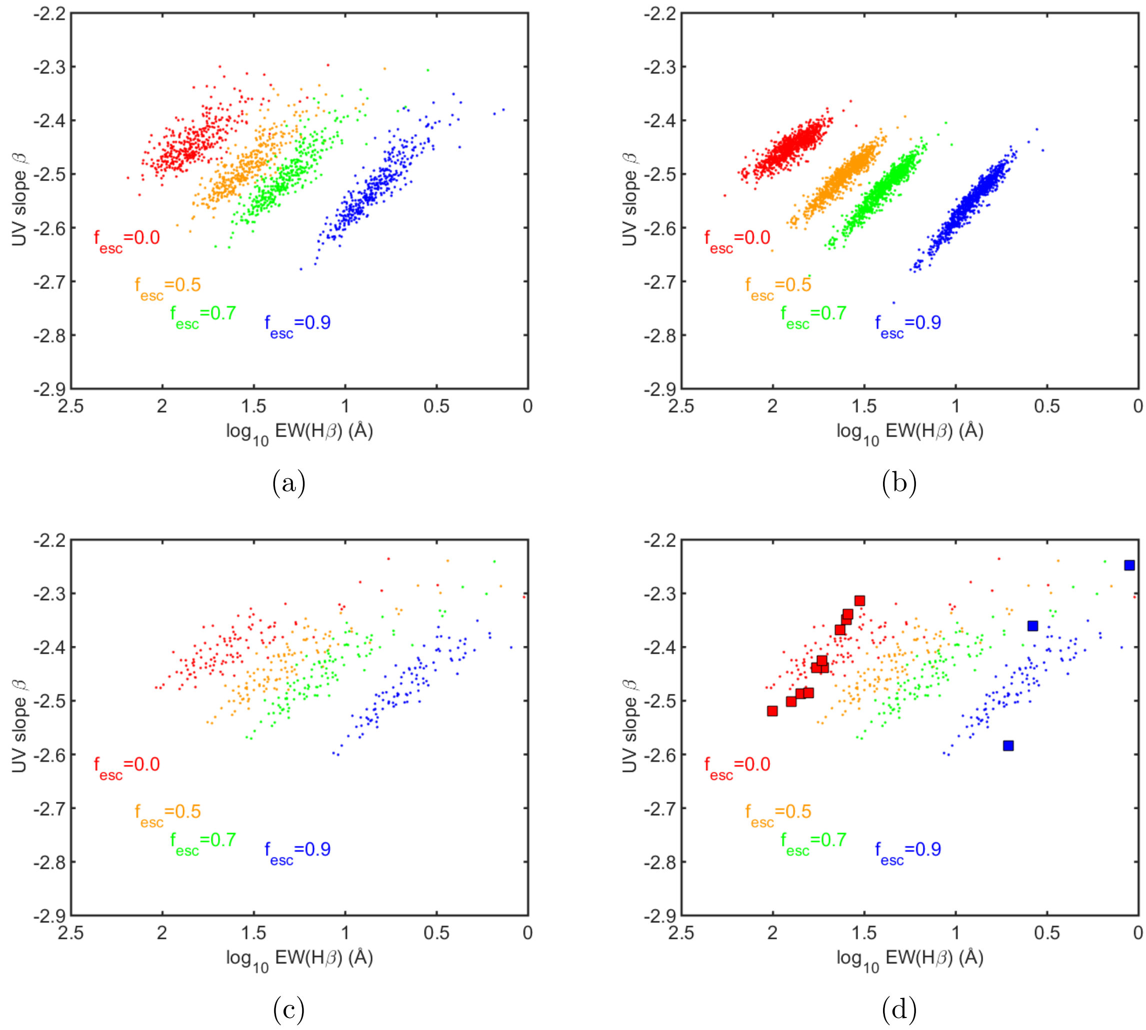

Figure 7: EW(Hβ)-β diagram showing all galaxies in the simulation sets for different escape fractions 0.0 (red), 0.5 (yellow), 0.7 (green) and 0.9 (blue). The different panels represent different simulations. *(a)* shows simulations by Shimizu et al. (2014) for galaxy masses $M_\star \geqslant 5 \times 10^8$ solar masses, *(b)* shows simulations by Gnedin (2014); Gnedin & Kaurov (2014) for galaxy masses $M_\star \geqslant 10^7$, *(c)* shows simulations by Finlator et al. (2013) for galaxy masses $M_\star \geqslant 10^7$ and *(d)* shows simulations by Paardekooper et al. (2013, 2015) for galaxy masses $M_\star \geqslant 10^7$ (Squares) on top of simulations by Finlator et al. (2013) for galaxy masses $M_\star \geqslant 10^7$. Note that in the case of the Paardekooper simulations, the escape fraction is predicted rather than assumed, and the squares are colored to match their escape fractions and placed on top of Finlators simulations to provide some reference points.

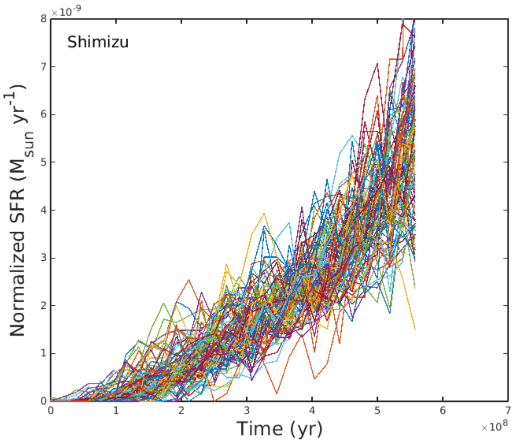

(a)

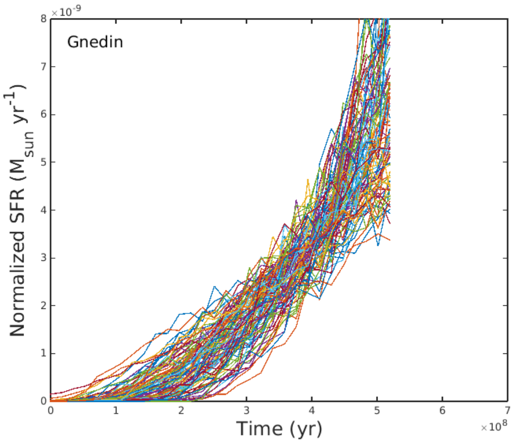

(b)

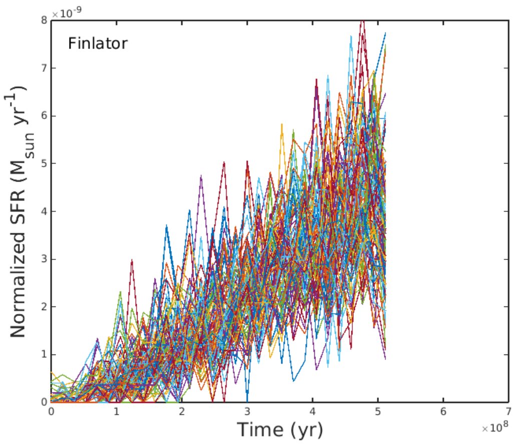

(c)

Figure 8: Star formation histories (SFH) for 100 galaxies at redshift $z \sim 7$ from the simulation sets. The different panels represent different simulations. *(a)* shows simulations by Shimizu et al. (2014) for galaxy masses $M_\star \geqslant 5 \times 10^8$ solar masses, *(b)* shows simulations by Gnedin (2014); Gnedin & Kaurov (2014) for galaxy masses $M_\star \geqslant 10^7$ solar masses, *(c)* shows simulations by Finlator et al. (2013) for galaxy masses $M_\star \geqslant 10^7$. The figure contains a high amount of galaxies to show the trend of the SFH, and that the simulations show different spreads.

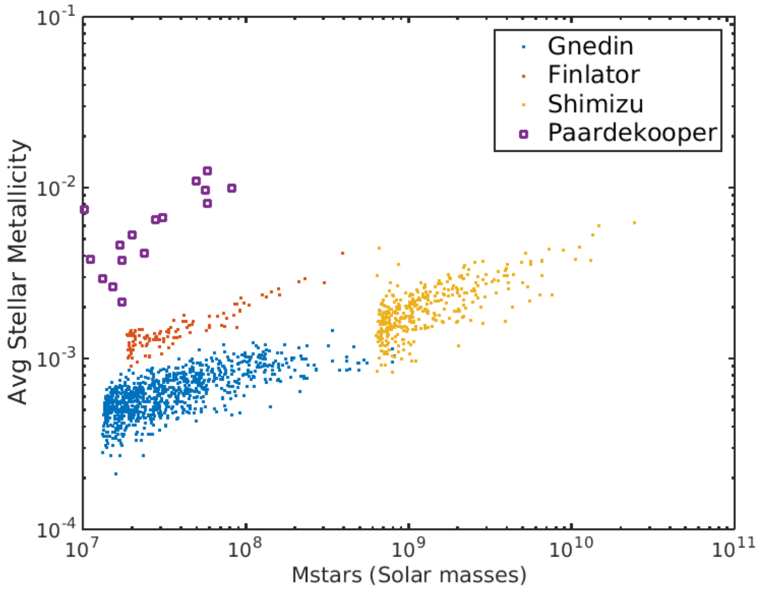

Figure 9: The metallicity distribution of the simulated galaxies. The plot shows the average metallicity versus the mass of all simulated galaxies for the Gnedin simulations *(blue)*, Finlator simulations *(brown)*, Shimizu simulations *(yellow)* and the Paardekooper simulations *(purple, squares)*. The galaxy masses are $M_\star \geqslant 10^7$ solar masses for the Finlator, Gnedin and Paardekooper simulations, while the Shimizu simulation has galaxy masses $M_\star \geqslant 5 \times 10^8$ solar masses.

overestimation of the nebular emission (Erb et al. 2006).

Originally, the Milky Way (MW) law by Pei (1992) was also included. However, due to the fact that the MW attenuation law has a bump in the UV part of the spectrum (figure 10), it was excluded. The bump appears in the wavelength region where the UV slope β is calculated, introducing an uncertainty into β. This bump is also observed in the Pei (1992) LMC law. However, the bump is not as prominent and should therefore not affect the calculation of β significantly.

4.2.1. The Finlator et al. (2006) dust recipe

In Finlator et al. (2006), the authors present a method to calculate the color excess $E(B-V)$ from metallicity using a correlation between reddening and metallicity observed in the Sloan Digital Sky Survey (SDSS) main galaxy sample. The mean color excess ($\langle E(B-V)\rangle$) is calculated for each galaxy using the metallicity of the galaxy (Z). A Gaussian scatter δE is added to the galaxy mean color excess. The variance of this Gaussian scatter is equal to one half of the mean color excess. This gives the relation

$$E(B-V) = \langle E(B-V)\rangle + \delta E, \quad \text{where } \langle E(B-V)\rangle = 9.0Z^{0.9} \tag{1}$$

Using the dust recipe by Finlator et al. (2006), the average (average over all galaxies)

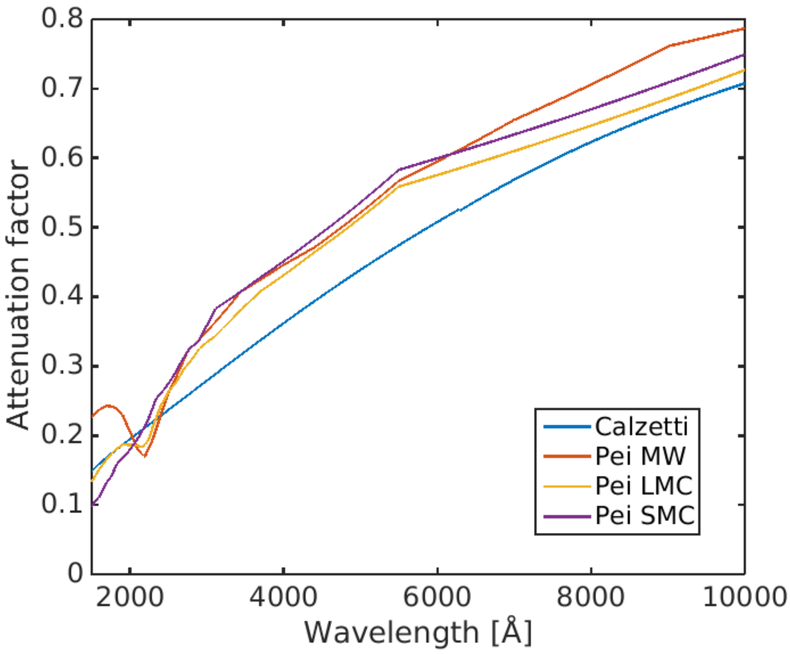

Figure 10: The different attenuation laws that are discussed when applying dust to the simulated galaxies. The figure shows the Stellar part of the Calzetti et al. (2000) attenuation curve *(blue)* and the Pei (1992) MW *(brown)*, LMC *(yellow)* and SMC *(purple)*. The MW curve was not used in this project due to the bump at ~ 2500 Å interfering with the calculation of the UV slope β. In this figure, a color excess $E(B-V) = 0.05$ was used. Note that the attenuation factor is the factor with which the flux is multiplied, so a smaller number means more attenuation.

color excess for the Finlator galaxies $\langle E(B-V) \rangle = 0.026$ which leads to a extinction in the V band of $A_v \approx 0.08 - 0.11$ depending on the attenuation law chosen. This lies in the range $A_v \lesssim 0.2$ mag. proposed by several studies (Finkelstein et al. 2012b; Bouwens et al. 2012a; Dunlop et al. 2012b; Wilkins et al. 2013).

In figure 11, the resulting EW(Hβ)-β diagram from using the Finlator et al. (2006) together with the attenuation laws (Calzetti et al. 2000; Pei 1992) for the Finlator simulation set can be seen. The addition of dust onto the galaxies makes the galaxies move toward flatter UV slopes, which is expected considering the reddening effect from interstellar dust.

The effect on the equivalent width of the Balmer β line is more subtle. The only attenuation law that has an impact on the equivalent width on the Balmer β line is the Calzetti et al. (2000) dust recipe. The reason for this is simply that the Calzetti attenuation law considers attenuation on the nebula and stellar component of the spectrum separately, and $E(B-V)_s = E(B-V)_n \cdot 0.44 \pm 0.03$, where $E(B-V)_s$ is the stellar color excess, and $E(B-V)_n$ is the nebular color excess. This means that the nebular component suffers more extinction than the stellar component, and thus the equivalent

Table 1: Effect on the average UV slope β of Finlator galaxies by different attenuation laws using the same average color excess $\langle E(B-V)\rangle$.

	$\langle A_v \rangle$ (mag)	$\langle E(B-V)\rangle$	$\langle \Delta\beta \rangle$
Calzetti 2000	0.2025	0.0500	0.2217
Pei 1996 LMC	0.1580	0.0500	0.3526
Pei 1996 SMC	0.1465	0.0500	0.5450

width of the emission lines from the nebula is diminished.

The correction for the dust could be done using the ratio of hydrogen lines $\frac{H_\beta}{H_\gamma}$, for which an attenuation A_v can be calculated. However, it seems that the dust attenuation is too small for us to be able to utilize the $\frac{H_\beta}{H_\gamma}$ ratio to correct for dust, simply because measuring the small change in the line ratios is not possible.

As discussed in section 3, since observations of galaxies in the reionization epoch seem to point toward an upper limit to the mean UV slope $\beta < -2$, we can use this to estimate the maximum color excess of the Finlator galaxies. Furthermore, the same upper limit can be used to estimate what the smallest equivalent width for the Balmer β line can be given the Calzetti et al. (2000) attenuation law. This test is performed by simply giving the same dust content to all galaxies, to see how large dust content is needed for the cloud of galaxies to reach an average UV slope equal to the limit. The upper limit on the average β slope $\langle\beta\rangle$ was reached for a color excess of $\langle E(B-V)\rangle = 0.09$ which corresponds to an attenuation in the visual $A_v \approx 0.36$ mag when using the Calzetti attenuation curve. What this means is that any higher dust content of the galaxies will lead to galaxies having an average β slope which is redder than $\beta = -2$, which seems to contradict observations. Using $\langle E(B-V)\rangle = 0.09$ leads to an average equivalent width of the Balmer β line $\langle EW(H\beta)\rangle = 32.3 - 3.1$ Å for escape fractions $f_{esc} = 0.0 - 0.9$. For the Balmer gamma line, the equivalent width becomes unmeasurable at escape fraction 0.9. The average equivalent width of the Balmer gamma line was calculated to $\langle EW(H\gamma)\rangle = 6.24 - 2.60$ Å for escape fractions $f_{esc} = 0.0 - 0.7$. The behaviour of the different curves for a given color excess $E(B-V)$ can be seen in table 1.

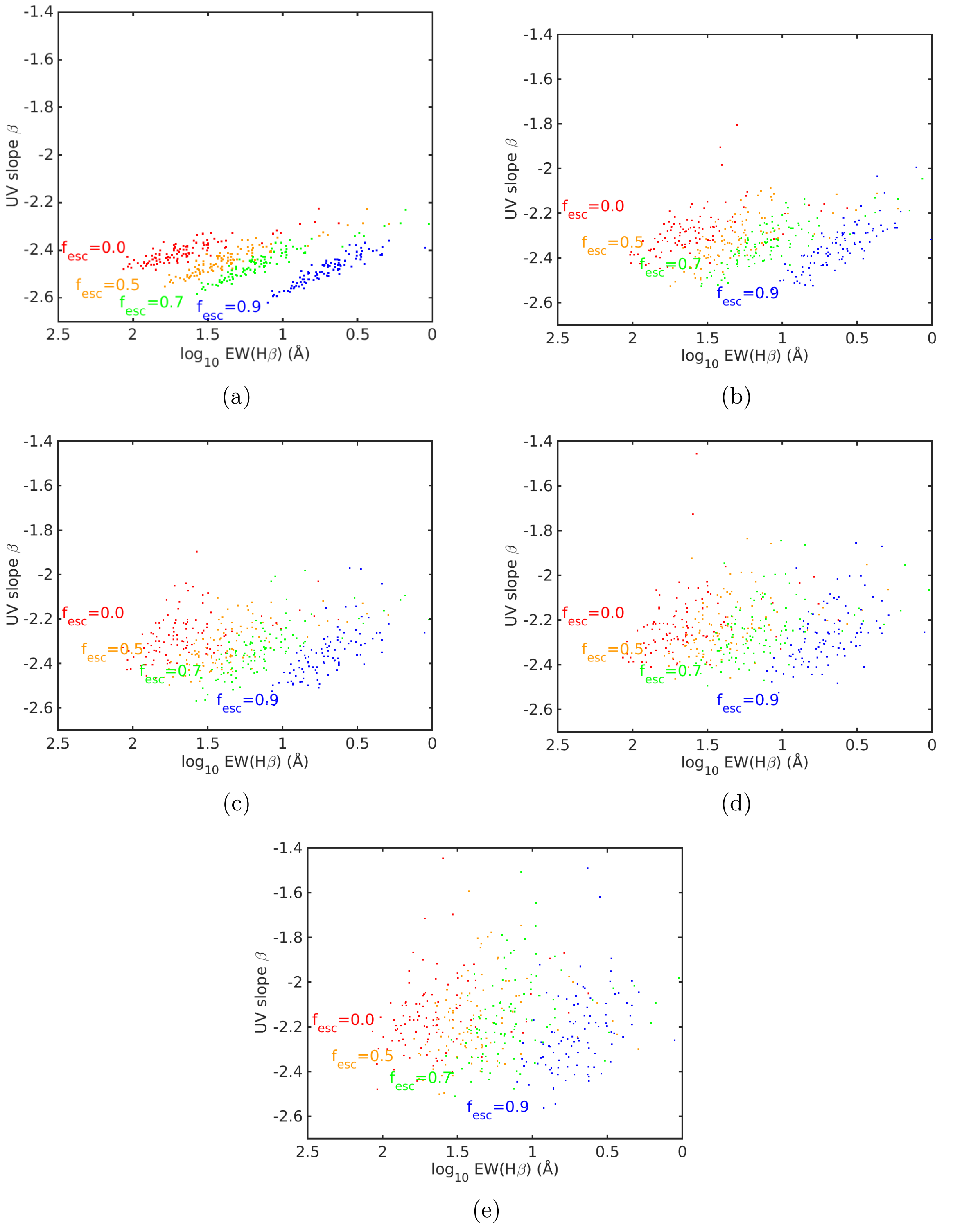

Figure 11: Positions of the simulated galaxies in the EW(Hβ)-β diagram for different escape fractions 0.0 (red), 0.5 (yellow), 0.7 (green) and 0.9 (blue). Simulations by Finlator for galaxy masses $M_\star \geqslant 10^7$ calculated while ignoring dust *(a)* and calculated using dust recipe by Finlator et al. (2006) and attenuation law by Calzetti et al. (2000) *(b)*, with same extinction for nebula and stellar part *(c)*, Large Magellanic Cloud *(d)* and Small Magellanic Cloud *(e)* attenuation laws by Pei (1992).

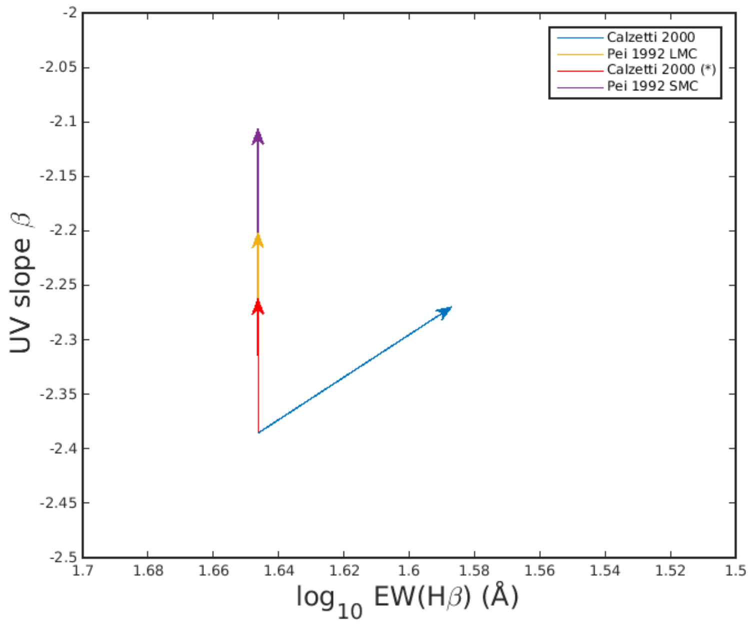

Figure 12: EW(Hβ) β diagram showing attenuation vectors for Calzetti et al. (2000) attenuation curve *(blue)* and the same law with same weights for the nebular and stellar attenuation *(red)*, and the Pei (1992) LMC *(yellow)* and SMC *(purple)*. Simulations by Finlator for one galaxy with mass $M_\star \approx 3.46 \times 10^7$ solar masses, with an average age of SPH particles at ≈ 167 Myr, absolute stellar metallicity $Z \approx 0.0015$. The extinction was calculated calculated using dust recipe by Finlator et al. (2006) yielding $E(B-V) \approx 0.026$ which leads to a maximum extinction of $A_v \approx 0.1$ mag.

4.2.2. Gaussian dust distributions

Dust was calculated using a Gaussian distribution of attenuation for different star particles of a galaxy. Here, spectra of 20 galaxies from the Gnedin simulations were used while considering a Gaussian distribution of color excess of each SPH particle. The color excess in this case is simply taken from a Gaussian distribution centered at $E(B-V) = 0.05$ and has a variance equal to half of that. In contrast to the dust recipe by Finlator et al. (2006), this recipe does not depend on metallicity. Furthermore, this recipe applies a different dust correction to each SPH particle rather than to the entire galaxy. The effect of this dust recipe on the EW(Hβ)-β diagram is shown in figure 13.

As expected, the addition of dust onto the Gnedin galaxies when using the Calzetti attenuation law leads to redder UV slopes and smaller equivalent widths of the Balmer beta line, as seen in the case of the Finlator et al. (2006) dust recipe (section 4.2.1). Since the dust is added without any consideration of the properties of a single star particle, it may be the case that by chance, particles with large EW(Hβ) get high attenuations, which suppresses the equivalent width of the Balmer beta line. The total effect may lead be a decrease of the EW(Hβ) of the galaxy. However, the opposite situation could also occur, where particles with large EW(Hβ) get little or no dust, while particles with small EW(Hβ) get high dust amounts. This could actually lead to an increase of the EW(Hβ) as the dust content is increased. However, the average effect on the cloud of galaxies should be representative of the effect of the dust recipe.

Again, using the upper limit set by observational studies, it is possible to calculate the largest average dust attenuation that the galaxies can have. Furthermore, the smallest equivalent widths of the Balmer lines can be calculated for the same case to give a lower limit for the equivalent widths. The upper limit of $\langle\beta\rangle \approx -2$ was reached for $\langle E(B-V)\rangle = 0.15$ ($A_v \approx 0.61$ when using the Calzetti attenuation curve) which leads to an average equivalent width of the Balmer β line $\langle EW(H\beta)\rangle = 46.8 - 5.2$ Å for escape fractions $f_{esc} = 0.0 - 0.9$. For the Balmer gamma line, the equivalent width becomes negative (unmeasurable) at escape fraction 0.9 due to an absorption feature in the spectrum. The average equivalent width of the Balmer gamma line was calculated to $\langle EW(H\gamma)\rangle = 14.1 - 1.1$ Å for escape fractions $f_{esc} = 0.0 - 0.7$.

The average effect of β depending on the dust attenuation can be seen in table 2. Note that these values were calculated using an average galaxy. The values can vary slightly depending on the Gaussian distribution and on how the different star particles get assigned different amounts of dust.

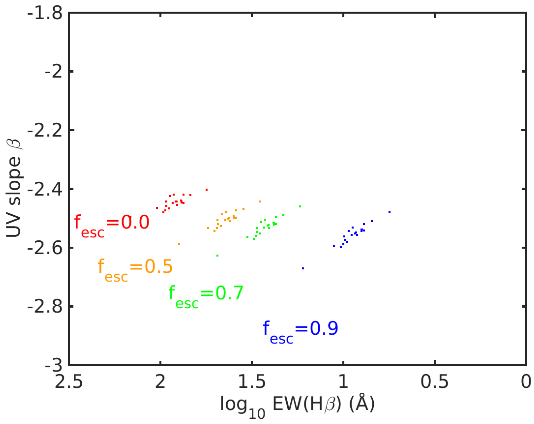

(a)

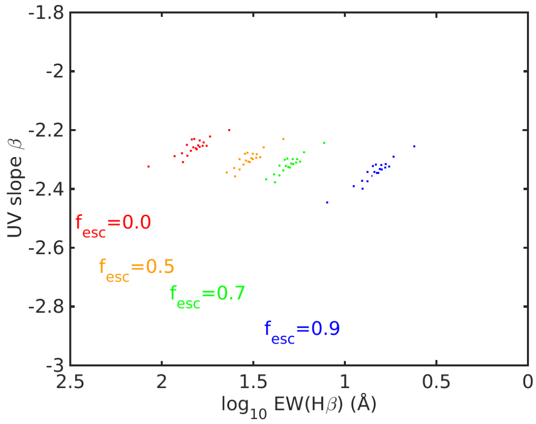

(b)

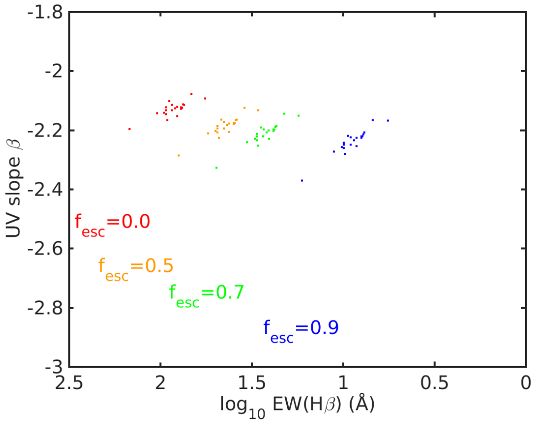

(c)

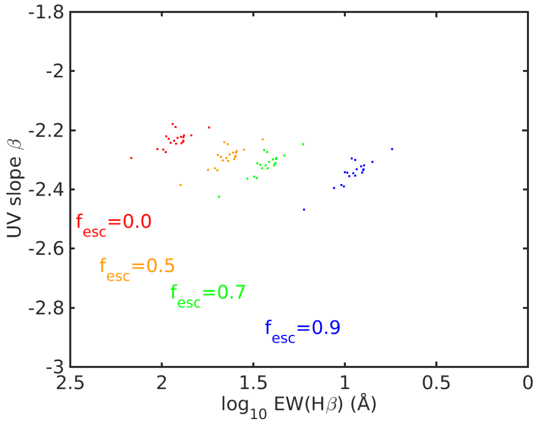

(d)

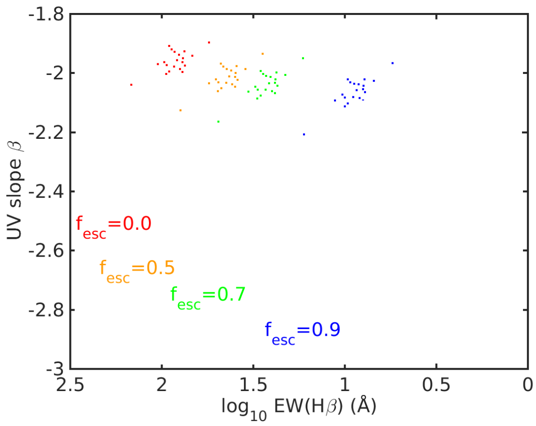

(e)

Figure 13: Positions of the simulated galaxies in the EW(Hβ)-β diagram for different escape fractions 0.0 (red), 0.5 (yellow), 0.7 (green) and 0.9 (blue). Simulations for 20 galaxies by Gnedin for galaxy masses $M_\star \geqslant 10^7$ calculated while ignoring dust *(a)* and calculated using a Gaussian dust distribution (section 4.2.2) and attenuation law by Calzetti et al. (2000) *(b)*, with same extinction for nebula and stellar part *(c)*, Large Magellanic Cloud *(d)* and Small Magellanic Cloud *(e)* attenuation laws by Pei (1992).

Table 2: Average effect on the UV slope β of Gendin galaxies by different attenuation laws using the same average color excess $\langle E(B-V)\rangle$ and the Gaussian dust distribution recipe.

	$\langle A_v\rangle$ (mag)	$\langle E(B-V)\rangle$	$\langle\Delta\beta\rangle$
Calzetti 2000	0.2025	0.0500	0.2022
Pei 1996 LMC	0.1580	0.0500	0.3184
Pei 1996 SMC	0.1465	0.0500	0.4897

4.2.3. The Bergvall et al. (2015) dust recipe

In Bergvall et al. (2015) the authors present a dust attenuation which depends on the age of the stellar component of a galaxy. The recipe is split into three age intervals (table 3), which leads to a different dust attenuation at different ages of the stellar components.

Table 3: Dust attenuation according to Bergvall et al. (2015) recipe

Age	Dust attenuation (mag)
$<$ 3 Myr	$(4.5 - \text{Age(Myr)}) \times A_0$
3 Myr $-$100 Myr	A_0
$>$ 100 Myr	$A_0/2$

In the connections in table 3, A_0 is the attenuation during the major period of star formation. In this thesis, a value of $A_0 = 0.3$ is assumed. The relation in table 3 was formulated to correct for dust in SDSS observations of galaxies in the local universe ($z \sim 0 - 0.25$) (Bergvall et al. 2015). The properties and dust content of nearby galaxies may not be at all similar to the properties and dust content of galaxies in the reionization epoch. Therefore, using this recipe in combination with simulations of high redshift galaxies risks produce galaxies that are not at all representative of those present during the reionization process. The result of applying the dust recipe to 35 galaxies from the Shimizu simulations can be seen in 14.

In contrast to the dust recipes discussed earlier, the Bergvall et al. (2015) recipe does significantly affect the equivalent width of the Balmer beta lines regardless of the attenuation law (see figure 15). The reason for this is most likely that dust is added to the star particles depending on their age, with older particles receiving less attenuation. This means that the youngest particles, which have the strongest LyC fluxes and therefore the largest EW(Hβ), experience the most attenuation, leading to an overall decrease in the equivalent width of the Balmer beta line.

The effect of a dust attenuation $A_0 = 0.3$ is quite large, and with this value, even the Calzetti curve leads to an average beta $\langle\beta\rangle \approx -2$. However, few particles actually experience high attenuation. The youngest particles in the set of 35 galaxies suffer an extinction of $A_v \approx 1.32$ and the mean age of the particles is generally higher than 100 Myr, with less than half of the number of particles with an actual age below 100 Myr. This means that the bulk of the particles will receive an attenuation which is lower than $A_v = 0.3$ (according to the connections presented in table 3).

The average equivalent widths of the Balmer lines using this attenuation with the Calzetti attenuation law were calculated to $\langle EW(H\beta)\rangle = 28.37 - 2.65$ and $\langle EW(H\gamma)\rangle = 8.03 - 0.27$ for escape fractions 0.0 and 0.9 respectively.

The effect of the dust attenuation on the average UV slope can be seen in table 4.

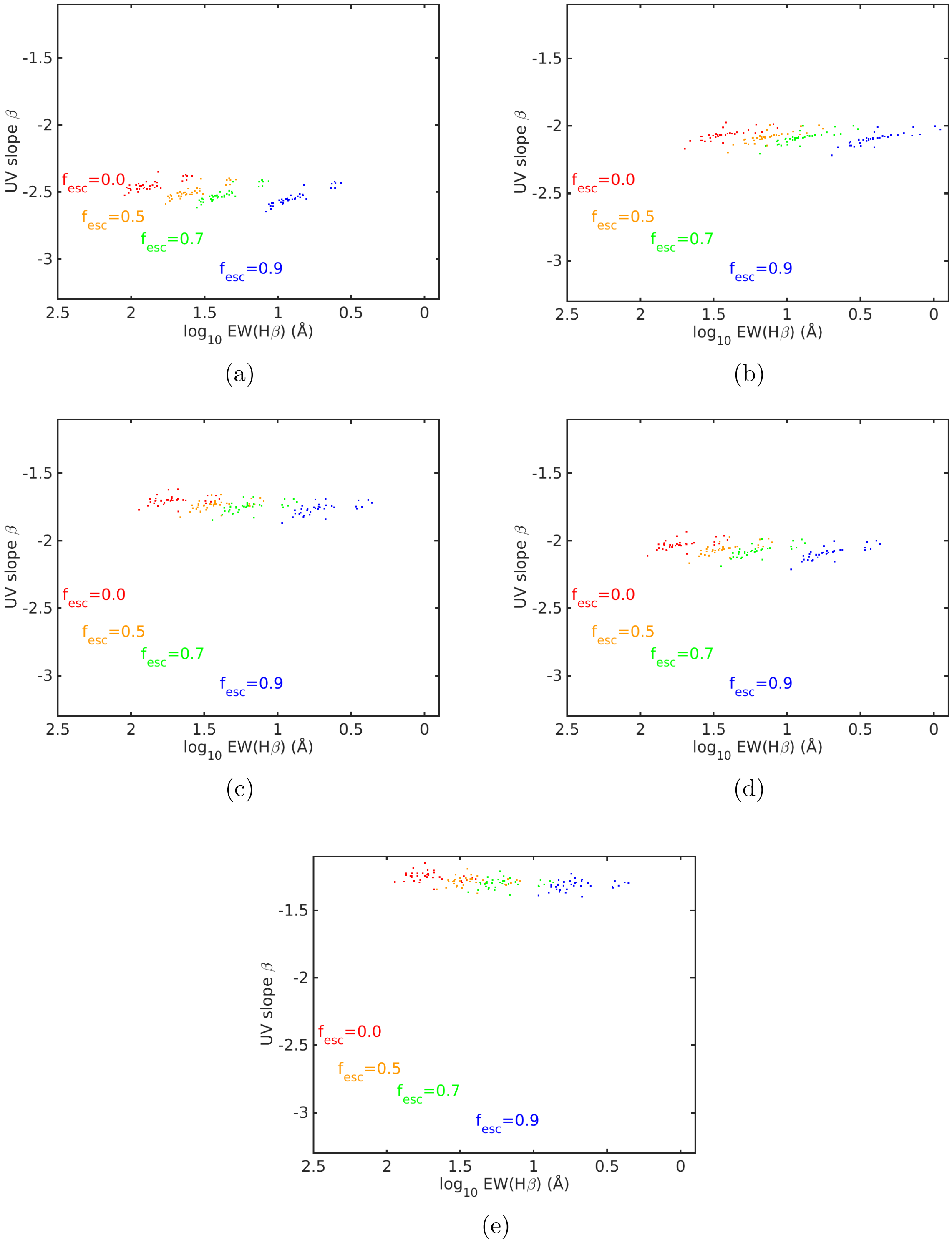

Figure 14: Positions of the simulated galaxies in the EW(Hβ)-β diagram for different escape fractions 0.0 (red), 0.5 (yellow), 0.7 (green) and 0.9 (blue). Simulations for 20 galaxies by Shimizu for galaxy masses $M_\star \geqslant 510^8$ calculated while ignoring dust *(a)* and calculated using the dust recipe by Bergvall et al. (2015) with $A_0 = 0.3$ and attenuation law by Calzetti et al. (2000) *(b)*, with same extinction for nebula and stellar part *(c)*, Large Magellanic Cloud *(d)* and Small Magellanic Cloud *(e)* attenuation laws by Pei (1992).

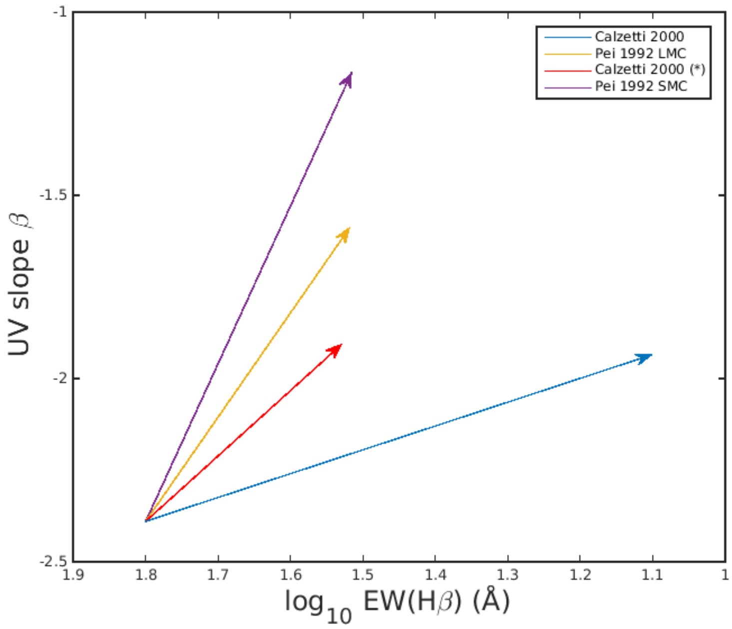

Figure 15: EW(Hβ) β diagram showing attenuation vectors for Calzetti et al. (2000) attenuation curve *(blue)* and the same law with same weights for the nebular and stellar attenuation *(red)*, and the Pei (1992) LMC *(yellow)* and SMC *(purple)*. Simulations by Shimizu for one galaxy with mass $M_\star \approx 1.32 \times 10^9$ solar masses and absolute stellar metallicity $Z \approx 0.0030$. The dust attenuation was calculated calculated using the Bergvall dust recipe using $A_0 = 0.3$.

Table 4: Average effect on the UV slope β of Shimizu galaxies by different attenuation laws using $A_0 = 0.3$ in the Bergvall et al. (2015) dust recipe.

	A_0 (mag)	$E(B-V)_0$	$\langle\Delta\beta\rangle$
Calzetti 2000	0.3	0.0741	0.3796
Pei 1996 LMC	0.3	0.0949	0.7296
Pei 1996 SMC	0.3	0.1024	1.2094

4.2.4. The Shimizu et al. (2014) dust recipe

Dust was added onto a new set of Shimizu model galaxies using the dust recipe presented in Shimizu et al. (2014). The resulting EW(Hβ)-β diagrams can be seen in figure 16. What can be seen is that this dust recipe significantly increases the spread of the galaxies in the EW(Hβ)-β diagram. The Shimizu recipe gives a mean UV slope of $\langle\beta\rangle \approx -2$ while using the Calzetti et al. (2000) attenuation law. This seems consistent with what is presented in Shimizu et al. (2014). Assuming the Calzetti attenuation curve, the mean attenuation for the was calculated to $\langle A_v\rangle \approx 0.4259$, which is similar to what is presented in Shimizu et al. (2014). For the Pei attenuation curves, this value becomes smaller.

As with the earlier recipes, this seems to point to a low dust content in the galaxies present at redshift $z \sim 7$. An estimation of the escape fraction of these galaxies is somewhat more problematic than in the earlier cases since the slope of the distribution of galaxies seems to change depending on dust recipe. For example, a very red galaxy with escape fraction $f_{esc} = 0.0$ calculated using the Calzetti attenuation could be mistaken for a galaxy with escape fraction $f_{esc} = 0.7$ calculated using the Pei SMC attenuation law. This introduces an ambiguity in the estimation of the escape fraction that cannot be resolved without assuming one of the attenuation laws for a given observed galaxy.

Using the Calzetti attenuation law leads to equivalent widths of Balmer lines of $\langle EW(H\beta)\rangle = 48.14 - 4.81$ and $\langle EW(H\gamma)\rangle = 15.81 - 1.34$ for escape fractions 0.0 to 0.9 respectively.

The Shimizu recipe does lead to a significant increase in the spread of the clouds of galaxies. However, the clouds are not moved significantly toward smaller EW(Hβ), except when the Calzetti attenuation law is used. In principle, this means that even though the effect seems large (as there is a large increase in spread), the estimation of the escape fraction is not strongly affected when using attenuation laws other than Calzetti.

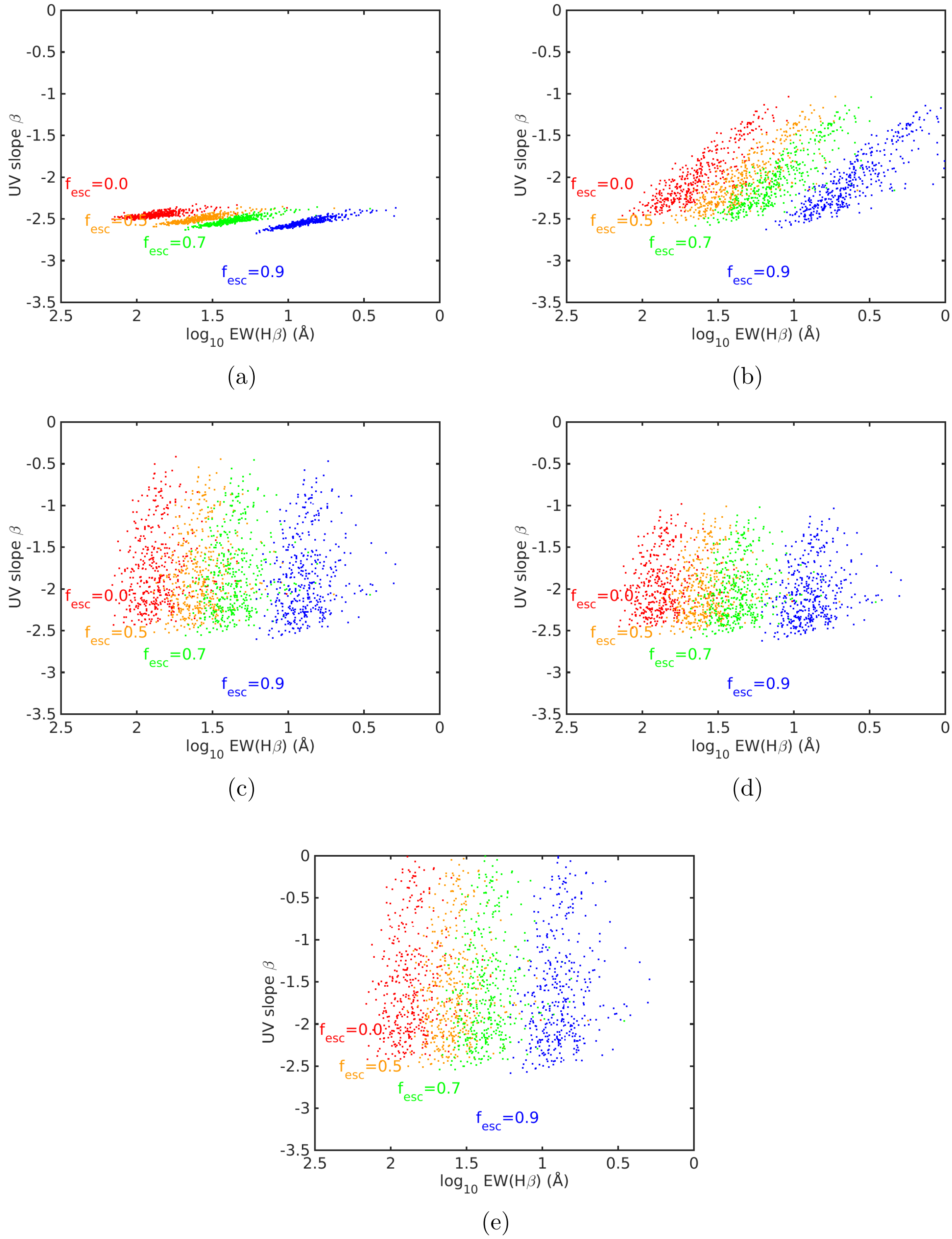

Figure 16: Positions of the simulated galaxies in the EW(Hβ)-β diagram for different escape fractions 0.0 (red), 0.5 (yellow), 0.7 (green) and 0.9 (blue). Simulations for ~ 400 galaxies by Shimizu for galaxy masses $M_\star \geqslant 510^8$ calculated while ignoring dust *(a)* and calculated using the dust recipe by Shimizu et al. (2014) and attenuation laws by Calzetti et al. (2000) *(b)*, with same extinction for nebula and stellar part *(c)*, Large Magellanic Cloud *(d)* and Small Magellanic Cloud *(e)* attenuation laws by Pei (1992).

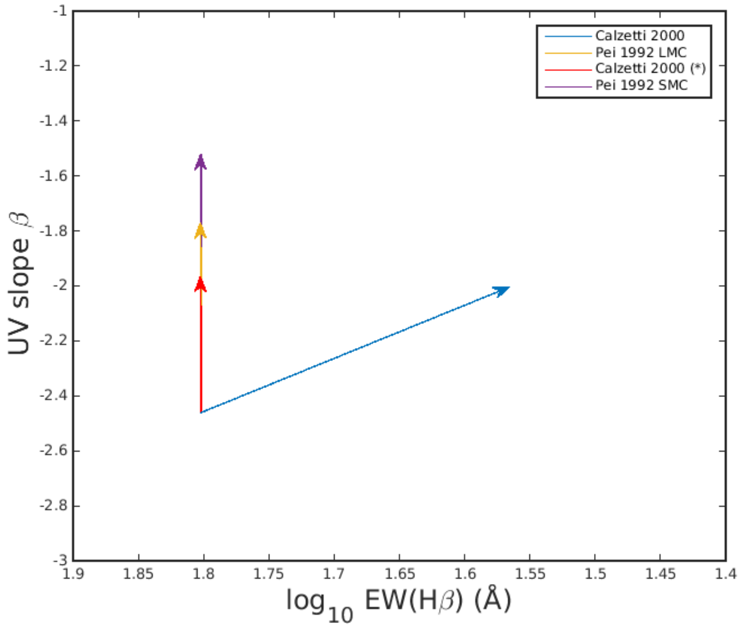

Figure 17: EW(Hβ) β diagram showing attenuation vectors for Calzetti et al. (2000) attenuation curve *(blue)* and the same law with same weights for the nebular and stellar attenuation *(red)*, and the Pei (1992) LMC *(yellow)* and SMC *(purple)*. Simulations by Shimizu for one galaxy with mass $M_\star \approx 2.27 \times 10^9$ solar masses and an absolute stellar metallicity $Z \approx 0.0019$. The dust attenuation was calculated calculated using the Shimizu dust recipe.

5. Conclusions

From the plots shown in section 4, it is clear that the technique discussed in this paper allows us to estimate the escape fraction of dust free simulated galaxies at redshift $z \sim 7$. The simulated galaxies form '*clouds*' in the shown EW(Hβ)-β diagram depending on their escape fraction. We should thus be able to estimate the escape fraction of a galaxy simply given its position in the diagram. Note that the technique only allows for an estimate, and as can be seen in figure 7, there may be an ambiguity in the estimation of escape fraction if a galaxy is positioned between the $f_{esc} = 0.5$ and the $f_{esc} = 0.7$ clouds. This is especially apparent in the Finlator simulations, where the two escape fraction clouds become mixed at larger β and smaller EW(Hβ). This means that the best case scenario is something like the Gnedin simulations, where the escape fraction can be quite accurately determined. However, a worst case scenario could only allow us to estimate if the escape fraction is high, low or intermediate.

In section 3, I discussed the effects of having different evolutionary tracks and choosing spectra in different ways. Throughout the thesis, I have used Geneva evolutionary tracks. However, I showed that choosing the Padova evolutionary tracks instead would produce significantly bluer galaxies. This should not have an effect on the effectiveness of the technique, but it may have an impact on the effect of dust, as I will discuss later. I showed that choosing spectra from Yggdrasil using three different methods (*'nearest neighbour'*, interpolation in metallicity/age and interpolation in log metallicity/age) produces very similar results. The choice of the method should therefore not impact the result of the technique in any significant way. Nonetheless, I have chosen to use the interpolation in log metallicity and log age method throughout this thesis.

The impact that dust has on the results is however significant. Dust was applied to the galaxies using four recipies and combining these with four different attenuation laws. As can be seen in figures 11, 13, 14 and 16, the positions of the galaxies in the EW(Hβ)-β diagram are strongly affected by the addition of dust onto the galaxies. In the above mentioned figures, it is clear that the dust can introduce an ambiguity to the escape fraction of the galaxies. In some cases, the galaxy clouds become mixed in such a way that the escape fraction determination is reduced to just determining whether a galaxy has a high or a low escape fraction. The figures 11, 13, 14 and 16 show that galaxies that have 'extreme' positions in the EW(Hβ)-β diagram (upper left or lower right corner) can be concluded to have either extremely low or extremely high escape fractions.

From the figures, it is possible to extract at what equivalent width galaxies can be concluded to have zero escape fraction. I found that galaxies with EW(Hβ)$\gtrsim 100$ Å are consistent with zero escape fraction. Of course, as the Bergvall et al. (2015) and Calzetti et al. (2000) move the galaxies toward smaller EW(Hβ), this limit also moves.

In principle, the $H\beta/H\gamma$ line ratio could be used to correct for this effect. However, the amount of dust in these galaxies was found to be too small to significantly affect the line ratio. Therefore, I was not able to apply a dust correction onto the galaxies. Other line ratios could have been used to correct for dust in these simulated galaxies, such as $H\beta/H\alpha$. However, this thesis discusses galaxies that should be possible to observe using the JWST NIRSpec instrument, and the $H\alpha$ line falls outside of the wavelength window of NIRSpec at $z \sim 7$ (Gardner et al. 2006). Furthermore, even if a dust correction could be applied, the situation would not completely solve the problem that dust introduces, since we do not know what attenuation law or dust recipe that best describes dust in real $z \sim 7$ galaxies. This means that the correction would have to be applied without considering the recipe and attenuation law that was used to add the dust. In the worst case scenario, the ambiguity introduced by the dust could remain. The best case scenario would of course be to move the galaxies back to their original positions.

Certain combinations of attenuation laws and dust recipes are particularly problematic. The extreme example of this is when the Bergvall et al. (2015) dust recipe is used in combination with the Calzetti et al. (2000) attenuation law. This combination leads to significantly smaller EW(Hβ) than the other recipes. The same effect is seen in any case where the Bergvall recipe or Calzetti law are used, but none as extreme as the combination of the two. This is somewhat problematic since small equivalent widths of the Balmer β line are used to identify the galaxies with highest escape fractions. The reason for this extreme shift in EW(Hβ) is that the Calzetti law applies a larger attenuation on the nebular part of the spectrum than the stellar part, which leads to a large attenuation for the nebular emission lines. The Bergvall recipe has basically the same effect. By giving younger star particles (the ones which still have a lot of gas and therefore a significant nebular component) a larger attenuation, galaxies with strong nebular emission become subject to more attenuation. The total effect of this is that nebular emission lines are affected more strongly than the stellar component of the spectrum. One may therefore question if using the Bergvall dust recipe and the Calzetti attenuation law together actually leads to physically plausible galaxies.

The Bergvall dust recipe was not designed for galaxies at these high redshifts, and it can also be questioned if the dust recipe is at all representative of dust in the reionization epoch. The recipe is based on the idea that the youngest star clusters have not yet been able to blow holes in or blow away the dust envelope surrounding them. However, the dust formation also depends on the metallicity of the galaxy. A galaxy at redshift $z \sim 7$ may not have had time to form metals in any large quantity, and therefore the young clusters may in fact be devoid of dust, or at least very dust-poor. This may lead to the Bergvall recipe being invalid for these early galaxies that were present during reionization.

The results from adding dust to the galaxies can be used to approximate the maximum dust content of the galaxies. Multiple studies point toward a UV slope $\beta \approx -2$ for $z \approx 7$ galaxies. Since β increases with dust content, it is possible to put an upper limit to the dust content of $z \sim 7$ galaxies by fitting the slope. Results from doing this point toward dust poor galaxies in the reionization epoch. The average dust content of the galaxies at redshift $z \sim 7$ can only be as high as $A_v \approx 0.4 - 0.6$ mag. Using the same fit, the lowest equivalent width of the Balmer lines could be calculated. The smallest equivalent width of the Balmer β line was found using the Bergvall dust recipe with the Calzetti attenuation law applied on a Shimizu simulated galaxy. The value was calculated to $\langle EW(H\beta)\rangle = 28.37 - 2.65$ Å for escape fractions 0.0 to 0.9. Corresponding equivalent widths for the Balmer γ lines were $\langle EW(H\gamma)\rangle = 8.03 - 0.27$ Å for the same galaxies. Values as small as 0.27 Å can be considered as unmeasurable. There are, however, smaller values for the γ lines when using other recipes (see section 4.2. When using the Finlator (section 4.2.1) and the normal dust distributions (section 4.2.2) at high escape fractions ($f_{esc} = 0.9$), the equivalent width of the Balmer γ line becomes negative due to an absorption feature.

To be able to determine the effects that dust actually have on the galaxies present during reionization, observations in the sub-millimeter range could be performed with for example the *Atacama Large Millimeter/submillimeter Array, ALMA*. These observations would then observe the reprocessed radiation that the dust is emitting. This could be used to further conclude if the galaxies during reionization did actually contain large amounts of dust. If no large amount of dust is observed, the results from this thesis could point toward how the galaxies behave in the case of little dust attenuation. If observations show signs of large amounts of dust, the $H\beta/H\gamma$ line from, for example NIRSpec data, could be used to correct for the dust.

There is a way that may allow us to reduce the uncertainty combined with choosing dust recipe and attenuation law for the high redshift galaxies. By using observations of intermediate and low redshift galaxies with similar properties, one could effectively calibrate the dust recipe and attenuation law for these types of galaxies. Of course, uncertainties will remain. It is not entirely clear if dust formation and distribution at low and intermediate redshifts is representative for galaxies at high redshifts.

An interesting way to follow up this project, and a possible way to solve the problems that dust introduces to the technique, would be to use additional spectral features to estimate the escape fractions and estimate the dust content. One especially exciting prospect is that of machine learning algorithms. If one could provide a computer with spectra for galaxies of different escape fractions and dust content (like the ones discussed in this thesis), it may be possible to use machine learning algorithms to '*teach*' the computer to identify galaxies of different escape fractions and different dust contents. This could lead to an evolved technique in which the whole spectrum and all spectral features available could be used. The estimation of the escape fraction and dust content could thus be done in a way that is impossible to a human being.

References

Adelberger, K. L. & Steidel, C. C. 2000, The Astrophysical Journal, 544, 218

Bergvall, N., Leitet, E., Zackrisson, E., & Marquart, T. 2013, Astronomy & Astrophysics, 554, A38

Bergvall, N., Marquart, T., Way, M. J., et al. 2015, arXiv:1501.06928 [astro-ph], arXiv: 1501.06928

Bergvall, N., Zackrisson, E., Andersson, B.-G., et al. 2006, Astronomy and Astrophysics, 448, 513

Borthakur, S., Heckman, T. M., Leitherer, C., & Overzier, R. A. 2014, Science, 346, 216

Bouwens, R. J., Illingworth, G. D., Franx, M., et al. 2009, The Astrophysical Journal, 705, 936

Bouwens, R. J., Illingworth, G. D., Oesch, P. A., et al. 2012a, The Astrophysical Journal, 754, 83

Bouwens, R. J., Illingworth, G. D., Oesch, P. A., et al. 2011, The Astrophysical Journal, 737, 90

Bouwens, R. J., Illingworth, G. D., Oesch, P. A., et al. 2014, The Astrophysical Journal, 793, 115

Bouwens, R. J., Illingworth, G. D., Oesch, P. A., et al. 2012b, The Astrophysical Journal Letters, 752, L5

Calzetti, D., Armus, L., Bohlin, R. C., et al. 2000, The Astrophysical Journal, 533, 682

Calzetti, D., Kinney, A. L., & Storchi-Bergmann, T. 1994, The Astrophysical Journal, 429, 582

Ciardi, B., Ferrara, A., & White, S. D. M. 2003, Monthly Notices of the Royal Astronomical Society, 344, L7

Clarke, C. & Oey, M. S. 2002, Monthly Notices of the Royal Astronomical Society, 337, 1299

Conroy, C. & Kratter, K. M. 2012, The Astrophysical Journal, 755, 123

Cowie, L. L., Barger, A. J., & Trouille, L. 2009, The Astrophysical Journal, 692, 1476

de Barros, S., Vanzella, E., Amorín, R., et al. 2015, arXiv:1507.06648 [astro-ph], arXiv: 1507.06648

Dunlop, J. S., McLure, R. J., Robertson, B. E., et al. 2012a, Monthly Notices of the Royal Astronomical Society, 420, 901

Dunlop, J. S., Rogers, A. B., McLure, R. J., et al. 2012b, arXiv:1212.0860 [astro-ph], arXiv: 1212.0860

Erb, D. K., Steidel, C. C., Shapley, A. E., et al. 2006, The Astrophysical Journal, 647, 128

Ferland, G. J., Korista, K. T., Verner, D. A., et al. 1998, Publications of the Astronomical Society of the Pacific, 110, 761

Fernandez, E. R., Dole, H., & Iliev, I. T. 2013, The Astrophysical Journal, 764, 56

Fernandez, E. R. & Shull, J. M. 2011, The Astrophysical Journal, 731, 20

Finkelstein, S. L., Papovich, C., Ryan, R. E., et al. 2012a, The Astrophysical Journal, 758, 93

Finkelstein, S. L., Papovich, C., Salmon, B., et al. 2012b, The Astrophysical Journal, 756, 164

Finlator, K. 2012, arXiv preprint arXiv:1203.4862

Finlator, K., Davé, R., Papovich, C., & Hernquist, L. 2006, The Astrophysical Journal, 639, 672

Finlator, K., Munoz, J. A., Oppenheimer, B. D., et al. 2013, Monthly Notices of the Royal Astronomical Society, 436, 1818

Gardner, J. P., Mather, J. C., Clampin, M., et al. 2006, Space Science Reviews, 123, 485

Gnedin, N. Y. 2014, The Astrophysical Journal, 793, 29

Gnedin, N. Y. & Kaurov, A. A. 2014, The Astrophysical Journal, 793, 30

Inoue, A. K., Shimizu, I., Iwata, I., & Tanaka, M. 2014, Monthly Notices of the Royal Astronomical Society, 442, 1805

Jaskot, A. E. & Oey, M. S. 2013, The Astrophysical Journal, 766, 91

Jones, T. A., Ellis, R. S., Schenker, M. A., & Stark, D. P. 2013, The Astrophysical Journal, 779, 52

Kravtsov, A. V., Klypin, A., & Hoffman, Y. 2002, The Astrophysical Journal, 571, 563

Kravtsov, A. V., Klypin, A. A., & Khokhlov, A. M. 1997, The Astrophysical Journal Supplement Series, 111, 73

Leitet, E., Bergvall, N., Hayes, M., Linné, S., & Zackrisson, E. 2013, Astronomy and Astrophysics, 553, A106

Leitet, E., Bergvall, N., Piskunov, N., & Andersson, B.-G. 2011, Astronomy and Astrophysics, 532, A107

Leitherer, C., Schaerer, D., Goldader, J. D., et al. 1999, The Astrophysical Journal Supplement Series, 123, 3

Leitherer, C., Vacca, W. D., Conti, P. S., et al. 1996, The Astrophysical Journal, 465, 717

Mac Low, M.-M. & McCray, R. 1988, The Astrophysical Journal, 324, 776

Mancini, M., Schneider, R., Graziani, L., et al. 2015, arXiv:1505.01841 [astro-ph], arXiv: 1505.01841

McLure, R. J., Dunlop, J. S., de Ravel, L., et al. 2011, Monthly Notices of the Royal Astronomical Society, 418, 2074

Ono, Y., Shimasaku, K., Dunlop, J., et al. 2010, The Astrophysical Journal, 724, 1524

Paardekooper, J.-P., Khochfar, S., & Dalla, C. V. 2013, Monthly Notices of the Royal Astronomical Society: Letters, 429, L94

Paardekooper, J.-P., Khochfar, S., & Vecchia, C. D. 2015, arXiv preprint arXiv:1501.01967

Pei, Y. C. 1992, The Astrophysical Journal, 395, 130

Pirzkal, N., Rothberg, B., Nilsson, K. K., et al. 2012, The Astrophysical Journal, 748, 122

Pirzkal, N., Rothberg, B., Ryan, R., et al. 2013, The Astrophysical Journal, 775, 11

Raiter, A., Schaerer, D., & Fosbury, R. A. E. 2010, Astronomy & Astrophysics, 523, A64

Robertson, B. E., Ellis, R. S., Dunlop, J. S., McLure, R. J., & Stark, D. P. 2010, Nature, 468, 49

Robertson, B. E., Ellis, R. S., Furlanetto, S. R., & Dunlop, J. S. 2015, The Astrophysical Journal Letters, 802, L19

Robertson, B. E., Furlanetto, S. R., Schneider, E., et al. 2013, The Astrophysical Journal, 768, 71

Rudd, D. H., Zentner, A. R., & Kravtsov, A. V. 2008, The Astrophysical Journal, 672, 19

Schaerer, D. & de Barros, S. 2010, Astronomy and Astrophysics, 515, A73

Shimizu, I., Inoue, A. K., Okamoto, T., & Yoshida, N. 2014, Monthly Notices of the Royal Astronomical Society, 440, 731

Shimizu, I., Yoshida, N., & Okamoto, T. 2011, Monthly Notices of the Royal Astronomical Society, 418, 2273

Shimizu, I., Yoshida, N., & Okamoto, T. 2012, Monthly Notices of the Royal Astronomical Society, 427, 2866

Siana, B., Shapley, A. E., Kulas, K. R., et al. 2015, The Astrophysical Journal, 804, 17

Springel, V. 2005, Monthly Notices of the Royal Astronomical Society, 364, 1105

Springel, V., Yoshida, N., & White, S. D. 2001, New Astronomy, 6, 79

Vanzella, E., de Barros, S., Castellano, M., et al. 2015, Astronomy and Astrophysics, 576, A116

Vázquez, G. A. & Leitherer, C. 2005, The Astrophysical Journal, 621, 695

Watson, D., Christensen, L., Knudsen, K. K., et al. 2015, Nature, 519, 327

Wilkins, S. M., Bunker, A., Coulton, W., et al. 2013, Monthly Notices of the Royal Astronomical Society, 430, 2885

Willott, C. J., Delorme, P., Reylé, C., et al. 2010, The Astronomical Journal, 139, 906

Zackrisson, E., Bergvall, N., & Leitet, E. 2008, The Astrophysical Journal Letters, 676, L9

Zackrisson, E., Inoue, A. K., & Jensen, H. 2013, The Astrophysical Journal, 777, 39

Zackrisson, E., Rydberg, C.-E., Schaerer, D., Östlin, G., & Tuli, M. 2011, The Astrophysical Journal, 740, 13

Zahn, O., Reichardt, C. L., Shaw, L., et al. 2012, The Astrophysical Journal, 756, 65